

Decoherence in Solid State Qubits

Luca Chirolli and Guido Burkard

Department of Physics, University of Konstanz, D-78457 Konstanz, Germany
 Institute of Theoretical Physics C, RWTH Aachen, D-52056 Aachen, Germany

(Received 00 Month 200x; In final form 00 Month 200x)

Interaction of solid state qubits with environmental degrees of freedom strongly affects the qubit dynamics, and leads to decoherence. In quantum information processing with solid state qubits, decoherence significantly limits the performances of such devices. Therefore, it is necessary to fully understand the mechanisms that lead to decoherence. In this review we discuss how decoherence affects two of the most successful realizations of solid state qubits, namely, spin-qubits and superconducting qubits. In the former, the qubit is encoded in the spin 1/2 of the electron, and it is implemented by confining the electron spin in a semiconductor quantum dot. Superconducting devices show quantum behavior at low temperatures, and the qubit is encoded in the two lowest energy levels of a superconducting circuit. The electron spin in a quantum dot has two main decoherence channels, a (Markovian) phonon-assisted relaxation channel, due to the presence of a spin-orbit interaction, and a (non-Markovian) spin bath constituted by the spins of the nuclei in the quantum dot that interact with the electron spin via the hyperfine interaction. In a superconducting qubit, decoherence takes place as a result of fluctuations in the control parameters, such as bias currents, applied flux, and bias voltages, and via losses in the dissipative circuit elements.

1 Introduction

1.1 *What is coherence? and why is it interesting?*

Coherence is a defining property of quantum mechanics. It can be argued that quantum coherence is the property that draws a line between the “quantum world” from the “classical world”. But what exactly is coherence? In physics, the term coherence refers to the property of waves to interfere, showing well known interference patterns. Two waves, depending on their relative phase, can produce a constructive interference, characterized by an enhancement of the amplitude of the wave, or destructive interference, accompanied by a complete suppression of it. Only the relative phase of the two waves makes the difference. To be precise we should therefore speak about phase coherence of quantum states.

By quantum states here we mean states of a quantum system, which in

turn can be constituted by more than one quantum object. The same rules of quantum mechanics that allow us to explain and predict interference of one object with itself, as the case of an electron through a double slit, predict that a system composed by two quantum subsystems can be in a state that has no classical counterpart, being a superposition with a precise phase of two or more quantum states of the whole system. This property of quantum states goes under the name of entanglement, and entangled states need to be phase coherent. In particular, coherence, as a property of quantum mechanical phenomena, disappears in the classical world, and it is therefore of fundamental interest to study it in theory and experiment. It is never completely possible to isolate a quantum system from the surrounding world. The system and its surrounding interact and, as a result, a randomization of the phase of the quantum system takes place, and the initial quantum state ends up in a classical state. This process is known as decoherence.

Only in recent years, thanks to the advances in technology, it has become possible to study quantum effects involving single quantum objects, like single photons, ions, electron spins, etc... Particular attention has been devoted to see coherence, from an experimental point of view, and to understand its limitation. In fact, though remarkable improvements have been achieved, nowadays, to see coherence, a lot of effort must be spent to understand how to preserve coherence. In the last decades, the idea of joining quantum physics laws and information science gave birth to a new and intriguing branch of science, quantum information theory, which studies the possibilities that quantum rules offer to information processing. In particular, the superposition principle opens the possibility to perform new and fast algorithms. The physical implementation of quantum information processing represents a challenge because one has to deal with the competition between fast and reliable quantum control, that requires interaction with the outside world, and good isolation of the quantum devices in order to ensure long coherence times.

Therefore, it is important to understand theoretically how decoherence happens in the systems under study (here, solid state systems) in order to make progress toward this ambitious goal (i.e. implementing quantum information).

1.1.1 *The quantum bit.* Classical information is based on binary logic, in which information is encoded in a series of bits (binary digits) that can assume only two values, 0 or 1. A typical example is a switch, with its two possible states “on” and “off”. All classical logical operations can be implemented as algorithms based on one- and two-bit operations, the so-called gates.

The building block of quantum information is the quantum bit, or qubit. Using the Dirac notation, the two states that characterize the qubit are $|0\rangle$ and $|1\rangle$ and they represent the quantum counterpart of the classical 0 and 1.

The most important property of a quantum bit is the possibility to be in a coherent superposition state

$$|\psi\rangle = \alpha|0\rangle + \beta|1\rangle, \quad (1)$$

with α and β complex numbers, characterized by a relative phase and by $|\alpha|^2 + |\beta|^2 = 1$. According to the postulates of quantum mechanics, $|\alpha|^2$ represents the probability for the qubit to be in the state $|0\rangle$, whereas $|\beta|^2$ represents the probability to be in $|1\rangle$. This means that if we prepare many copies of the same system in the state $|\psi\rangle$, a measurement of the state of the qubit will produce the outcome 0 with rate $|\alpha|^2$, and the outcome 1 with rate $|\beta|^2$. In which case the two logical states are the spin up $|\uparrow\rangle$ and the spin down $|\downarrow\rangle$. The two states $|0\rangle$ and $|1\rangle$ form a basis of the Hilbert space $\mathcal{H} = \text{span}\{|0\rangle, |1\rangle\}$ of the qubit.

A good example of a qubit is the spin 1/2. In order to explain the necessity to use complex number α and β to characterize the state of the qubit, we describe an interference procedure for a spin 1/2 particle. Suppose we prepare the spin in the state $|\psi_0\rangle = |\uparrow\rangle$, that is with probability 1 to find it parallel with respect to a certain direction z in the space, that we choose as quantization axis. We then rotate the spin by an angle $\pi/2$ about an axis perpendicular to z , i.e. the y axis. The result is the state

$$|\psi_1\rangle = e^{-i\frac{\pi}{4}\sigma_y}|\uparrow\rangle = \frac{1}{\sqrt{2}}(|\uparrow\rangle + |\downarrow\rangle). \quad (2)$$

We then let the spin cross a region in which there is a magnetic field that points in the positive z direction, $\mathbf{B} = (0, 0, B)$. Due to the presence of the magnetic field, the two states $|\uparrow\rangle$ and $|\downarrow\rangle$ accumulate a relative phase 2φ , that depends on the magnitude of the magnetic field and the time t spent in the region with the \mathbf{B} field, and that for simplicity we leave unspecified. Up to an overall phase, the state of the system that comes out from the region with a magnetic field is given by

$$|\psi_2\rangle = \frac{1}{\sqrt{2}}(|\uparrow\rangle + e^{2i\varphi}|\downarrow\rangle). \quad (3)$$

Now, we again rotate the spin of $\pi/2$ about the y direction, and obtain

$$|\psi_3\rangle = e^{-i\frac{\pi}{4}\sigma_y}|\psi_2\rangle = e^{i\varphi}[\cos(\varphi)|\uparrow\rangle + i\sin(\varphi)|\downarrow\rangle]. \quad (4)$$

If we now measure the state of the spin, we obtain $|\uparrow\rangle$ with probability $\cos^2(\varphi)$ and $|\downarrow\rangle$ with probability $\sin^2(\varphi)$. We clearly see, now, that the relative phase

can really affect the state of a quantum system. This procedure is known as Ramsey interference [1] and it is used in experiments to detect coherent oscillations in the transverse spin component.

1.1.2 One qubit as environment. Decoherence is a consequence of the interaction of the qubit with the surrounding environment. As an instructive example we consider the case in which the environment is constituted by another qubit. For the Hamiltonian describing the interaction between the two qubits we choose ($\hbar = 1$)

$$H = \frac{J}{4} \sigma_1^z \otimes \sigma_2^z, \quad (5)$$

where the operator $\sigma_1^z \otimes \sigma_2^z$ is a two-qubit operator, given by the tensor product of two single-qubit operators, and it acts in the tensor product space $\mathcal{H} = \mathcal{H}_1 \otimes \mathcal{H}_2$. We note that our general argument does not depend on the specific form of H , as long as it describes an interaction between the qubits. As the initial state for the two qubit system we choose a product state $|+\rangle_1 \otimes |+\rangle_2$, where the single qubit state is $|+\rangle = (|0\rangle + |1\rangle)/\sqrt{2}$, written in the basis diagonal with respect to σ_z , $\sigma_z|0\rangle = |0\rangle$, and $\sigma_z|1\rangle = -|1\rangle$. We let the system evolve according to the unitary evolution generated by the Hamiltonian Eq. (5) for a time t , after which we perform a trace operation on the second qubit and have a look how the state of the first qubit evolved during the time t in which it has interacted with the second qubit. We re-write the initial state of the first qubit as a pure state density matrix, $\rho_1 = |+\rangle_1 \langle +|$. In the $\{|0\rangle, |1\rangle\}$ basis it is found to be

$$\rho_1(0) = \frac{1}{2} \begin{pmatrix} 1 & 1 \\ 1 & 1 \end{pmatrix}. \quad (6)$$

The state of the two qubit system after a time t is given by $|\psi(t)\rangle = U(t)|++\rangle$, with $U(t) = \exp(-iJt\sigma_1^z\sigma_2^z/2)$. After some algebra the state of the first qubit at time t is given by

$$\rho_1(t) = \text{Tr}_2[|\psi(t)\rangle\langle\psi(t)|] = \frac{1}{2} \begin{pmatrix} 1 & \cos(Jt/2) \\ \cos(Jt/2) & 1 \end{pmatrix}. \quad (7)$$

The diagonal element of the first qubit density matrix is left unchanged by the interaction with the second qubit, whereas the off-diagonal elements change in time. The coherence of a state is encoded in the off-diagonal element of the density matrix. After a time $t = \pi/J$ the coherence is completely lost (full decoherence). However, due to the smallness of the environment considered,

the first qubit periodically recovers its original state. It is therefore clear that the interaction with the environment strongly affects the qubit coherence.

1.2 Quantum open systems

According to the axioms of quantum mechanics the dynamics of a closed conservative system is described as a unitary time evolution. In such a picture the system is considered to be decoupled from the surrounding environment, that does not influence at all the dynamics of the closed system. Strictly speaking this is never the case. However, under certain conditions the coupling to the environment can be considered to be weak, and to a good approximation neglected.

In condensed phases, the coupling to the environment can be relatively strong, and the system under consideration cannot be separated from its surrounding. However, often a rather complex physical situation can be modelled by a system that consists of few dynamical variables in contact with a huge environment, constituted by a very large or even infinite number of degrees of freedom. In this case the small relevant system alone has to be described as an open system.

Generally, an open system is a quantum system S which is coupled to an other quantum system B called the environment. It can therefore be thought to be a subsystem of the combined system $S + B$, which in turn in many cases is considered to be a closed system, governed by Hamiltonian dynamics. The system S will in turn change according to its internal dynamics, and as a consequence of the interaction with the environment. Certain system-environment correlations will be established between the two parts and, as a consequence, the dynamics of a quantum open system cannot, in general, be described in terms of a unitary time evolution.

Denote \mathcal{H}_S the Hilbert space of the system S , and \mathcal{H}_B the Hilbert space of system B . The dynamics of the combined system $S + B$ takes place in the Hilbert space given by the tensor product space $\mathcal{H}_{SB} = \mathcal{H}_S \otimes \mathcal{H}_B$. The total Hamiltonian can be chosen to have the general form

$$H = H_S + H_B + H_I, \quad (8)$$

where H_S describes the evolution of the system S alone, H_B is the free Hamiltonian of the environment B , and H_I describes the interaction between the system and the environment. Usually when speaking about the *environment* of the system S , the term *reservoir* may appear, that refers to an environment with an infinite number of degrees of freedom, such that the frequency modes associated with it form a continuum spectrum. Occasionally the term *heat bath* or simply *bath* refers to a reservoir which is in thermal equilibrium.

The presence of an environment is meant to model the communication of the open system with the external world. However the attention is focused on the subsystem under study S , and all observations of interest refer to the subsystem S . Formally this means that all observables of interest act on the Hilbert space \mathcal{H}_S . Denoting the state of the total system by ρ , the expectation values of all observables may be written as

$$\langle \mathcal{O} \rangle = \text{Tr}_S [\mathcal{O} \rho_S], \quad \rho_S = \text{Tr}_B [\rho], \quad (9)$$

where \mathcal{O} is the Hermitian operator describing the observable, ρ_S is the reduced density matrix of the open system S , and $\text{Tr}_{S(B)}$ denotes a partial trace on the system $S(B)$.

All informations that describe the open system S are contained in the reduced density matrix ρ_S . Since the total system evolves unitarily in time, $\rho_S(t)$ is obtained as partial trace over the environment B of $\rho(t)$,

$$\rho_S(t) = \text{Tr}_B \left[U(t, t_0) \rho_S(t_0) U^\dagger(t, t_0) \right], \quad (10)$$

where $U(t, t_0)$ is the unitary evolution operator of the total system. The equation of motion for the open system reduced density matrix $\rho_S(t)$ is

$$\frac{d}{dt} \rho_S(t) = -i \text{Tr}_B [H(t), \rho_S(t)]. \quad (11)$$

1.3 Generalized master equation

In many cases it is useful to model the dynamics of an open system by means of an appropriate equation of motion for its density matrix, the so called quantum master equation. The evolution in time of the total system ρ is governed by the well known Liouville equation of motion

$$\dot{\rho} = -i[H(t), \rho(t)] \equiv -i\mathcal{L}\rho(t), \quad (12)$$

where the second equality defines the Liouville operator \mathcal{L} . As the Hamiltonian can be divided into three terms that describe the dynamics of the two systems alone, H_S and H_B , and a interaction between the two parts, H_I , the Liouville operator can be written as the sum of three contributions

$$\mathcal{L} = \mathcal{L}_S + \mathcal{L}_B + \mathcal{L}_I. \quad (13)$$

Without going into details that are beyond the scope of this review, we just mention the fact that the Liouvillian is a superoperator, that maps operators

into operators. The initial state for the combined system $S + B$ can typically be chosen to be a product state, $\rho(0) = \rho_S(0) \otimes \rho_B$.

We have already introduced the reduced density matrix ρ_S of the open subsystem S . It can be formally obtained from the density matrix of the total system ρ by means of a projection operation, that contains a partial trace over the system B ,

$$\rho_S = \mathcal{P}\rho = \text{Tr}_B[\rho] \otimes \rho_B. \quad (14)$$

Here, ρ_B is a fixed density matrix for the environment. Mapping operators into operators, the projector \mathcal{P} is also a superoperator. We may thus decompose the ρ as

$$\rho(t) = \rho_S(t) + (1 - \mathcal{P})\rho(t), \quad \mathcal{P}^2 = \mathcal{P}. \quad (15)$$

Substituting this decomposition in the Liouville equation of motion for the total system Eq. (12), choosing the projector in such a way that the inhomogeneous term that depends on the initial state can be disregarded, and using that the operator \mathcal{P} defined in Eq. (14) commutes with the Liouvillian of the open system \mathcal{L}_S , after some algebra, the equation of motion for the reduced density matrix $\rho_S(t)$ can be cast in the form of an exact generalized master equation, the *Nakajima-Zwanzig equation* [2, 3]

$$\dot{\rho}_S(t) = -i\mathcal{L}_S\rho_S(t) + \int_0^t dt' \Sigma(t-t')\rho_S(t'), \quad (16)$$

$$\Sigma(t)\rho_S = -i\text{Tr}_B \left[\mathcal{L}_I e^{(1-\mathcal{P})\mathcal{L}t} \mathcal{L}_I \rho_S \otimes \rho_B \right], \quad (17)$$

where $\Sigma(t)$ is the self-energy superoperator. The first term describes the reversible evolution of open system S , while the second term produces irreversibility.

1.3.1 Born approximation. The generalized master equation Eq. (16) is a formally exact and closed description of the dynamics of the state of the system ρ_S , but it is very complicated from a mathematical point of view and rather unpractical. Usually, in order to handle it and some approximation are made. In fact, the kernel of Eq. (16) contains all powers of \mathcal{L}_I , and the dynamics of ρ_S at time t depends on the whole history of the density matrix. If the coupling between system and reservoir is weak, i.e. $\|\mathcal{L}_I\| \ll \|\mathcal{L}_S + \mathcal{L}_B\|$, the exponential can be expanded in power of \mathcal{L}_I in a perturbative way. In lowest order Born approximation, the interaction Liouvillian is disregarded in

the exponent and \mathcal{L}_I is retained only to second order

$$\tilde{\Sigma}(t)\rho_S = -i\text{Tr}_B \left[\mathcal{L}_I e^{(1-\mathcal{P})(\mathcal{L}_S + \mathcal{L}_B)t} \mathcal{L}_I \rho_S \otimes \rho_B \right]. \quad (18)$$

The applicability of the master equation in the Born approximation is strictly restricted to those cases in which the coupling between system and environment is weak, with decoherence and relaxation times large compared to the relevant time scales of the reversible dynamics.

1.4 Quantum Markov process

The master equation in the Born approximation Eq. (18), though it is much simpler than the exact Nakajima-Zwanzig equation (16), is still an integro-differential equation that is very difficult to handle. Assuming that the temporal correlations in the bath are short lived and typically lead to exponential decay of the coherence and populations, the master equation in the Born approximation Eq. (18) can be further simplified. In the Born-Markov approximation the master equation for the reduced density matrix of system S assumes the form

$$\dot{\rho}_S(t) = -i\mathcal{L}_S \rho_S(t) + \tilde{\Sigma}^R(t)\rho_S(t), \quad (19)$$

$$\tilde{\Sigma}^R(t) = -i \int_0^t dt' \tilde{\Sigma}(t') e^{it' \mathcal{L}_S}. \quad (20)$$

In an eigenstate basis of H_S , the master equation in the Born-Markov approximation can be written as the so called Redfield equation [4–6]

$$\dot{\rho}_{nm} = -i\omega_{nm}\rho_{nm}(t) - \sum_{k,l} R_{nmkl}\rho_{kl}(t), \quad (21)$$

where $\rho_{nm} = \langle n | \rho_S | m \rangle$, $\omega_{nm} = \omega_n - \omega_m$, and we have introduced the Redfield tensor

$$R_{nmkl} = \int_0^\infty dt \text{Tr}_B \left[\langle n | [H_I^{\text{int}}(t), [H_I^{\text{int}}(0), |k(t)\rangle \langle l(t)| \rho_B]] | m \rangle \right], \quad (22)$$

where we have used the interaction picture Hamiltonian and the system eigenstates in the interaction picture

$$H_I^{\text{int}}(t) = e^{i(H_S + H_B)t} H_I e^{-i(H_S + H_B)t}, \quad |k(t)\rangle = e^{iH_S t} |k\rangle = e^{i\omega_k t} |k\rangle. \quad (23)$$

The first term of Eq. (21) represents the reversible motion in terms of the transition frequencies ω_{nm} , while the second term describes relaxation. The Redfield tensor can be expressed as

$$R_{nmkl} = \delta_{nm} \sum_r \Gamma_{nrrk}^{(+)} + \delta_{nk} \sum_r \Gamma_{lrrm}^{(-)} - \Gamma_{lmnk}^{(+)} - \Gamma_{lmnk}^{(-)}, \quad (24)$$

in terms of rates given by the golden rule expression

$$\Gamma_{lmnk}^{(+)} = \int_0^\infty dt e^{-i\omega_{nk}t} \text{Tr}_B \left[\tilde{H}_I(t)_{lm} \tilde{H}_I(0)_{nk} \rho_B \right], \quad (25)$$

$$\Gamma_{lmnk}^{(-)} = \int_0^\infty dt e^{-i\omega_{lm}t} \text{Tr}_B \left[\tilde{H}_I(0)_{lm} \tilde{H}_I(t)_{nk} \rho_B \right], \quad (26)$$

with $\tilde{H}_I(t)_{lm} = \langle n | e^{itH_B} H_I e^{-itH_B} | m \rangle$, and $(\Gamma_{lmnk}^{+})^* = \Gamma_{lmnk}^{-}$.

We have already pointed out that the dynamics of an open system cannot be described as a unitary evolution. However, the mapping describing the evolution is required to be completely positive [7], implying $\rho \rightarrow \sum_n O_n \rho O_n^\dagger$, where $\{O_n\}$ is a set of linear operators on the reduced state space that satisfy $\sum_n O_n^\dagger O_n = 1$, such to preserve the trace of ρ . In the framework of Lindblad theory [7], the master equation can be cast in the form

$$\dot{\rho}(t)_S = -i[H_S, \rho_S(t)] + \frac{1}{2} \sum_j \left\{ [L_j \rho_S(t), L_j^\dagger] + [L_j, \rho_S(t) L_j^\dagger] \right\}. \quad (27)$$

The Lindblad operators L_j describe the effect of the environment in the Born-Markov approximation.

1.4.1 Two level systems and Bloch equations. The aim of this review is to provide an overview on the mechanisms that affect qubit dynamics and induce decoherence in solid state realizations of qubits. Therefore we concentrate on two level systems and their coupling to the surrounding environment.

The density operator of a two state system is a two dimensional positive Hermitian operator with trace one. It can thus be expressed in terms of a basis of Hermitian operators given by the three Pauli operators $\boldsymbol{\sigma} = (\sigma_x, \sigma_y, \sigma_z)$ and the 2×2 identity,

$$\rho = \frac{1}{2}(1 + \mathbf{p} \cdot \boldsymbol{\sigma}), \quad \mathbf{p} = \text{Tr}[\rho \boldsymbol{\sigma}] = \begin{pmatrix} \rho_{01} + \rho_{10} \\ i(\rho_{01} - \rho_{10}) \\ \rho_{00} - \rho_{11} \end{pmatrix}. \quad (28)$$

The vector \mathbf{p} is known as the Bloch vector, and for a spin-1/2 object it represents the expectation values of the spin components $\mathbf{p}/2 \equiv \langle \mathbf{S} \rangle = \text{Tr}[\mathbf{S}\rho]$, where $\mathbf{S} = \boldsymbol{\sigma}/2$, with σ_z diagonal in the $|0\rangle$ $|1\rangle$ basis, $\sigma_z|0\rangle = |0\rangle$ and $\sigma_z|1\rangle = -|1\rangle$. Combining the last equation with the Redfield equation (21) in the case that $n, m, k, l = 0, 1$, the master equation within the Born-Markov approximation for the density matrix of a two level system can be expressed as a first order time differential equation for the expectation value of the spin component $\langle \mathbf{S} \rangle = (\langle S_x \rangle, \langle S_y \rangle, \langle S_z \rangle)$,

$$\langle \dot{\mathbf{S}} \rangle = \boldsymbol{\omega} \times \langle \mathbf{S} \rangle - R \langle \mathbf{S} \rangle + \langle \mathbf{S}_0 \rangle, \quad (29)$$

with $\boldsymbol{\omega} = (0, 0, \omega_{01})$. In case of a spin 1/2 particle in a magnetic field defining the z direction, ω_{01} represents the Zeeman splitting. The inhomogeneous term $\langle \mathbf{S}_0 \rangle$ and the relaxation matrix R depend on the rates Eqs. (25), (26). If $\omega_{01} \gg R_{nmkl}$, it is possible to make a secular approximation, retaining only terms R_{nmkl} with $n - m = k - l$, [8], such that the Redfield tensor can be approximated by the diagonal form

$$R \approx \begin{pmatrix} T_2^{-1} & 0 & 0 \\ 0 & T_2^{-1} & 0 \\ 0 & 0 & T_1^{-1} \end{pmatrix}, \quad (30)$$

where the relaxation time T_1 and the decoherence time T_2 are given by

$$\frac{1}{T_1} = 2\text{Re}(\Gamma_{0110}^{(+)} + \Gamma_{1001}^{(+)}), \quad (31)$$

$$\frac{1}{T_2} = \frac{1}{2T_1} + \frac{1}{T_\phi}, \quad (32)$$

with the pure dephasing time T_ϕ , given by

$$\frac{1}{T_\phi} = \text{Re}(\Gamma_{0000}^{(+)} + \Gamma_{1111}^{(+)} - 2\Gamma_{0011}^{(+)}). \quad (33)$$

For a system-environment coupling given by a simple bilinear form $H_I = \mathcal{O}_S \otimes \mathcal{X}_B$, with \mathcal{O}_S an operator acting in the system space \mathcal{H}_S , and \mathcal{X}_B an operator acting in the environment space \mathcal{H}_B , the relaxation and dephasing

times T_1 and T_ϕ can be written as

$$\frac{1}{T_1} = 4|\langle 0|\mathcal{O}_S|1\rangle|^2 J(\omega_{01}) \coth \frac{\omega_{01}}{2k_B T}, \quad (34)$$

$$\frac{1}{T_\phi} = |\langle 0|\mathcal{O}_S|0\rangle - \langle 1|\mathcal{O}_S|1\rangle|^2 \left. \frac{J(\omega)}{\omega} \right|_{\omega \rightarrow 0} 2k_B T, \quad (35)$$

where the spectral density $J(\omega)$ is the Fourier transform of the environment time correlator

$$J(\omega) = \int_{-\infty}^{\infty} dt \text{Tr}_B [\mathcal{X}_B \mathcal{X}_B(t) \rho_B] e^{-i\omega t}. \quad (36)$$

The first term in Eq. (29) produces a rotation of the Bloch vector along the z direction. If $R = 0$ we have the classical picture of a magnetic moment precessing along the externally applied magnetic field. The second term proportional to R describes an exponential damping of the component of the Bloch vector. T_1 describes the decay of the longitudinal component of the Bloch vector, while T_2 describes the decay of the transverse component.

We remark that the Markovian results Eq. (32) satisfy the expected fundamental Korringa relation [9].

1.5 Spin-boson model

Here we describe a simple model to treat the dynamics of a two-level system in contact with a reservoir. We consider a generic two-level system described by the Hamiltonian

$$\mathcal{H}_S = \frac{\Delta}{2} \sigma_x + \frac{\epsilon}{2} \sigma_z. \quad (37)$$

In order to include the effect of dissipation in the quantum formalism, it is customary to follow the Caldeira-Leggett [10–12] approach. A bath of harmonic oscillators at thermal equilibrium at temperature T is introduced to describe the degrees of freedom of the environment. The system+bath Hamiltonian is

$$H = H_S + H_B + H_{SB}, \quad (38)$$

$$H_B = \frac{1}{2} \sum_{\alpha} \omega_{\alpha} \left(b_{\alpha}^{\dagger} b_{\alpha} + \frac{1}{2} \right), \quad (39)$$

$$H_{SB} = \mathcal{O}_S \otimes \mathcal{X}_B = \sigma_z \sum_{\alpha} c_{\alpha} \left(b_{\alpha} + b_{\alpha}^{\dagger} \right), \quad (40)$$

where \mathcal{H}_S is the quantized Hamiltonian of the system Eq. (37), \mathcal{H}_B is the bath Hamiltonian, described by independent bosonic degrees of freedom with frequencies ω_α . The coupling between the system and the bath degrees of freedom is described by \mathcal{H}_{SB} , where $\mathcal{O}_S = \sigma_z$, $\mathcal{X}_B = \sum_\alpha c_\alpha (b_\alpha + b_\alpha^\dagger)$, and c_α are coupling parameters.

A rigorous treatment of the spin-boson model in the Born approximation without making use of the Markov approximation is presented in [13,14]. The eigenstates of the Hamiltonian Eq. (37) are

$$|0\rangle = \frac{1}{\sqrt{2}} \left(\sqrt{1 + \frac{\epsilon}{\omega_{01}}} |+\rangle + \sqrt{1 - \frac{\epsilon}{\omega_{01}}} |-\rangle \right), \quad (41)$$

$$|1\rangle = \frac{1}{\sqrt{2}} \left(\sqrt{1 - \frac{\epsilon}{\omega_{01}}} |+\rangle - \sqrt{1 + \frac{\epsilon}{\omega_{01}}} |-\rangle \right), \quad (42)$$

where $|\pm\rangle$ are eigenstates of σ_z , $\sigma_z|\pm\rangle = \pm|\pm\rangle$, and $\omega_{01} = \sqrt{\Delta^2 + \epsilon^2}$. The initial state of a system of quantum harmonic oscillators in thermal equilibrium is

$$\rho_B = \mathcal{Z}_B^{-1} \exp(-\beta\mathcal{H}_B), \quad \mathcal{Z}_B = \text{Tr} \exp(-\beta\mathcal{H}_B). \quad (43)$$

All the informations of the bath, such as the bath frequencies ω_α and the coupling parameters c_α appearing in the Hamiltonian, are contained in the spectral density $J(\omega)$ of the system-bath coupling,

$$J(\omega) = \frac{\pi}{2} \sum_\alpha c_\alpha^2 \delta(\omega - \omega_\alpha). \quad (44)$$

Here we limit our attention to the Markovian case, and make use of the general Redfield theory described in the previous section. From the formula Eqs. (34), (35), the relaxation and dephasing rates take the form

$$\frac{1}{T_1} = \left(\frac{\Delta}{\omega_{01}} \right)^2 J(\omega_{01}) \coth \frac{\omega_{01}}{2k_B T}, \quad (45)$$

$$\frac{1}{T_\phi} = \left(\frac{\epsilon}{\omega_{01}} \right)^2 \frac{J(\omega)}{\omega} \Big|_{\omega \rightarrow 0} 2k_B T. \quad (46)$$

1.6 Spin qubits

Per antonomasia, the two-state system that nature provides us with is the intrinsic angular momentum of the electron: the spin 1/2. It is therefore natural

to choose the electron spin as the two-state system that encodes the qubit. The spin of the electron can have much longer decoherence time than the charge degrees of freedom. Nevertheless, isolating the spin degree of freedom of an electron to a degree required for quantum computation is not at all an easy task. Moreover, in order to be used for quantum computational purposes, electron spin-based qubits must be designed as scalable devices that can be externally controlled, coupled, manipulated, and read-out, i.e. they must satisfy the DiVincenzo criteria [15]. A successful and promising device for the physical implementation of electron spin-based qubits is the semiconductor quantum dot [16].

1.7 *Semiconductor quantum dots*

The quantum dots owe their name to the zero-dimensional character of such devices. Can be considered as a quantum box that can be filled with electrons (or holes) which occupy the available discretized states of the system. The electrons can tunnel on and off the dot, which is coupled to large reservoir via tunnel barriers. The height of the barriers, and consequently the rates for tunneling through the barriers on and off the dot, can be controlled via the application of gate electrodes. Electrostatic gates can also be used to tune the electrostatic potential of the dot with respect to the reservoirs, such that the ladder of energy levels in the dot can be shifted up or down with respect to the energy of the reservoir. External bias voltages can be applied and transport properties can be measured.

Quantum dots are basically characterized by the quantized level structure, for which they are considered as artificial atoms, and by the transport state of the dot, that can be active or blocked, and depends on the combination of bias and gate voltages applied. In fact, the Coulomb repulsion between the electrons in the dot determines an energy cost for adding an extra electron in the dot. At low temperatures, the tunneling of electrons on and off the dot can be drastically suppressed, and the dot is in the so called Coulomb blockade.

Many kinds of quantum dots have been realized so far. Here we focus the attention on lateral III-V semiconductor quantum dots, as those in Fig. 1. These devices are fabricated from heterostructures of GaAs and AlGaAs grown by molecular beam epitaxy. The energy potential along the growth direction of such a structure has a minimum at the interface of the two layers, which is also asymmetric with respect to the growth direction. Free electrons are introduced by doping the AlGaAs layer with Si, which accumulate at the GaAs/AlGaAs interface, deep down in the minimum of the vertical potential, that provides strong confinement of the electrons along the growth direction. At the same time, the electrons are free to move along the interface, where they form a two dimensional electron gas (2DEG), that can have a high mobility and a

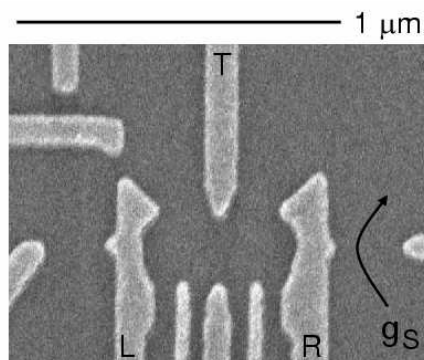


Figure 1. Scanning electron micrograph of a double quantum dot. [17] (With permission from the Authors).

relatively low electron density (typically $10^5 - 10^7 \text{ cm}^2/\text{Vs}$ and $\approx 10^{15} \text{ m}^{-2}$). The low density results in a relatively long Fermi wavelength ($\approx 40 \text{ nm}$) and a large screening length, such that via application of an electric field, obtained through metal gate electrodes on top of the heterostructure negatively charged, the 2DEG can be locally depleted. Therefore, by suitable designing the gate structure it is possible to isolate small islands of the 2DEG, thus creating a dot. When the lateral size of the dot is compared to the Fermi wavelength, the energy level structure of the dot becomes discretized, and at temperatures down to tens of mK, the energy separation of the levels becomes much higher than the temperature, such that quantum phenomena start to play a significant role.

1.8 *Spin relaxation and spin dephasing mechanisms in quantum dots*

The electron spin in semiconductor quantum dots can be isolated and controlled with a high accuracy, but it still suffers from decoherence due to the unavoidable coupling with the surrounding environment. In order to implement quantum computation algorithms with electron spin-based qubits in semiconductor quantum dots, it is necessary to engineer the devices in such a way to preserve the coherence of the electron spin states for sufficiently long time scales. Besides the fundamental interest, it is therefore important to theoretically understand which sources of dissipation and decoherence affect the electron spin in quantum dots, and to find ways to reduce their influence on the spin-qubit dynamics as much as possible.

Two kinds of environment turn out to mainly affect the dynamics of an electron spin in a quantum dot, the phonons in the lattice, and the spins of atomic nuclei in the quantum dot.

Phonon-induced relaxation in semiconductor quantum dots has attracted some attention from a theoretical point of view for the first time in [18, 19]. The lattice phonons do not couple directly to the spin degree of freedom. However, even without the application of external electric fields, the breaking of inversion symmetry in GaAs gives rise to spin-orbit interaction, that couples the spin and the orbital degrees of freedom. The latter, being coupled to the phonons, provide an indirect coupling between the electron spin and the phonons, that constitute a large dissipative bosonic reservoir and provide a source of decoherence and relaxation. Short time correlations in the phonon bath induce a Markovian dynamics of the electron spin, with well defined relaxation and decoherence time T_1 and T_2 . It turns out that effectively the phonon-induced pure dephasing time T_ϕ of an electron spin in a quantum dot in the presence of a magnetic field diverges. In the Bloch picture, pure dephasing arise from longitudinal fluctuations of the magnetic field, while a perturbative treatment of the spin-orbit interaction gives rise, within first order, to a fluctuating magnetic field perpendicular to the applied one. As a consequence the decoherence time T_2 is limited only by its upper bound T_1 , $T_2 = 2T_1$. In turn the relaxation time T_1 shows a strong dependence on the magnetic field, $T_1 \propto B^5$, that has been confirmed experimentally, where a very long relaxation time up to $T_1 \approx 1$ s has been measured for a magnetic field of $B = 1$ T [21].

Hyperfine interaction was for the first time taken into consideration as a source of decoherence for an electron spin confined in a quantum dot in [22]. In GaAs there are $\approx 5 \times 10^{21}$ atoms in 1 cm^3 . Therefore, the linear extension of a typical GaAs quantum dot, that is of order of the Fermi wavelength ≈ 40 nm, encompasses roughly 200 atoms, from which it can be estimated that the wavefunction of an electron in a GaAs quantum dot overlaps with $\approx 10^5$ nuclei. The electron spin and the nuclear spins in the dot couple via the Fermi contact hyperfine interaction, that creates entanglement between them and strongly affect the electron spin dynamics. It turns out that long time correlations in the nuclear spin system induce a non-Markovian dynamics of the electron spin, with non exponential decay in time of the expectation values of the electron spin components. In a large applied magnetic field B , the dynamics in the nuclear field due to the hyperfine interaction can be treated perturbatively and it turns out that flip-flop dynamics starts to affect the nuclear field in a time that scales like the number of nuclear spins, $\propto N$. For shorter times the nuclear field is static and the transverse component shows a Gaussian decay, that is due to the statistical distribution of nuclear spin states.

We remark that the phonon induced relaxation rate of the electron spin is enhanced by an applied magnetic field, whereas the influence of the hyperfine interaction is reduced by a large Zeeman splitting.

1.9 Hyperfine-induced decoherence in spin qubits

1.10 Hyperfine interaction

The spin of an electron and the atomic nuclear spin can interact through the hyperfine Fermi contact interaction, a spin-spin interaction that takes place when the electron and the nucleus occupy the same position in space, from which the term “contact”. The origin of the hyperfine coupling can be understood considering the electromagnetic interaction of an electron with the magnetic field produced by a nucleus. Without loss of generality the magnetic properties of a nucleus can be described as those of a magnetic dipole $\boldsymbol{\mu}_N = \mu_N \hbar \mathbf{I}$, where μ_N is the nuclear magneton, and \mathbf{I} is the nuclear spin operator. The interaction of a nuclear dipole $\boldsymbol{\mu}_N$ with the electronic shell gives a rather small effect, and can be treated using a perturbative method. In the non-relativistic Pauli description of the electron, the Hamiltonian of an electron in a magnetic field $\mathbf{B} = \nabla \times \mathbf{A}$ produced by a vector potential \mathbf{A} is given by

$$\mathcal{H} = \frac{1}{2m} \left(\mathbf{p} + \frac{e}{c} \mathbf{A} \right)^2 + 2\mu_B \mathbf{S} \cdot (\nabla \times \mathbf{A}), \quad (47)$$

where \mathbf{S} is the electron spin operator. The vector potential produced by a magnetic dipole $\boldsymbol{\mu}$ at position \mathbf{r} is, according to classical electromagnetism, $\mathbf{A} = (\boldsymbol{\mu} \times \mathbf{r})/r^3 = \nabla \times (\boldsymbol{\mu}/r)$. Neglecting the term quadratic in the vector potential and replacing $\hbar \mathbf{L} = \mathbf{r} \times \mathbf{p}$ for the electron orbital momentum operator, the Hamiltonian Eq. (47) can be written as

$$\mathcal{H} = 2\mu_B \frac{\mathbf{L} \cdot \boldsymbol{\mu}}{r^3} + 2\mu_B (\mathbf{S} \cdot \nabla) (\boldsymbol{\mu} \cdot \nabla) \frac{1}{r} - 2\mu_B (\mathbf{S} \cdot \boldsymbol{\mu}) \nabla^2 \frac{1}{r}. \quad (48)$$

The magnetic interaction of the nuclear spin and the electron spin is contained in the second and the third term of Eq. (48), and it is obtained after integration over the orbital degrees of freedom, i.e. it has to be understood as applied to an electron orbital state $\psi_{\text{el}}(\mathbf{r})$. For $\mathbf{r} \neq 0$, the terms involving the electron spin \mathbf{S} in Eq. (48) behave regularly, the last term vanishes identically, while the second term produces a usual dipole-dipole interaction $2\mu_B [3(\mathbf{S} \cdot \mathbf{r})(\boldsymbol{\mu} \cdot \mathbf{r})/r^5 - \mathbf{S} \cdot \boldsymbol{\mu}/r^3]$. The case $\mathbf{r} = 0$ needs to be treated more carefully. It can be shown [9] that the dominant contribution of the spin dependent part of Eq. (48) reduces to $(16\pi/3)\mu_B (\mathbf{S} \cdot \boldsymbol{\mu}) \delta(\mathbf{r})$, and once applied on the electron orbital wave function is given by

$$\mathcal{H}_{\text{hy}} = \frac{16}{3} \pi \mu_B |\psi_{\text{el}}(0)|^2 \mathbf{S} \cdot \boldsymbol{\mu}, \quad (49)$$

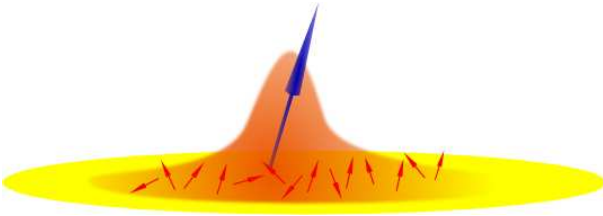


Figure 2. Schematic representation of the orbital wave function of an electron in a quantum dot. Due to the spatial extension of the wave function, the electron spin (big blue arrow) couples to many nuclear spins (small red arrows).

which is finite for s electrons and zero for others. The Hamiltonian for the magnetic interaction of the electron with the nucleus can be written as

$$\mathcal{H} = 2\mu_B\mu_N\hbar\mathbf{I} \cdot \left[\frac{\mathbf{L}}{r^3} - \frac{\mathbf{S}}{r^3} + 3\frac{\mathbf{r}(\mathbf{S} \cdot \mathbf{r})}{r^5} + \frac{8}{3}\pi\mathbf{S}\delta(\mathbf{r}) \right]. \quad (50)$$

1.10.1 Hyperfine interaction in semiconductor quantum dots. In a semiconductor quantum dot an electron is confined in a 2D region of space whose linear extension is of the order of the Fermi wavelength, for GaAs about $\sim 100\text{nm}$, that is much larger than the typical lattice spacing of the crystal ($\sim \text{\AA}$). As a result a discretization of the energy levels in the dot appears, with an orbital level spacing that, for lateral quantum dot containing single electrons, is much greater than the typical energy scale of the hyperfine interaction. As opposed to the case of single atoms, the electron orbital wave function in a quantum dot extends over a region much larger than the lattice size, such that the electron spin couples to many nuclear spins, as schematically shown in Fig. 2. The effective hyperfine Hamiltonian describing the interaction of a single electron with the nuclei in the dot can be written as

$$\mathcal{H} = \mathbf{S} \cdot \mathbf{h}, \quad \mathbf{h} = Av_0 \sum_{k=1}^N |\psi_0(\mathbf{r}_k)|^2 \mathbf{I}_k \equiv \sum_{k=1}^N A_k \mathbf{I}_k, \quad (51)$$

where \mathbf{S} is the electron spin operator, \mathbf{h} is the so-called Overhauser field, given by the sum of all the \mathbf{I}_k nuclear spin operators, weighted by the position dependent coupling strength $A_k = v_0 A |\psi_0(\mathbf{r}_k)|^2$, where the square modulus of the electron envelope wave function at the k th lattice site. Typically the electron can be assumed to be in the quantum dot orbital ground state. v_0 is the volume of the crystal unit cell containing one nuclear spin and $A = 16\pi\mu_B\mu_N\hbar/3$ is the contact hyperfine coupling strength. In GaAs the nuclear spin is $I = 3/2$ and an estimate of the interaction strength, weighted by the

abundances of the three isotopes naturally present (^{69}Ga , ^{71}Ga , and ^{75}Ga), yields $A \approx 90\mu\text{eV}$.

The inhomogeneity of the electron wave function results in a nonuniform hyperfine coupling strength A_k , that depends on the probability to find the electron in the nuclear lattice site k , resulting in a subtle and complex many-body quantum mechanical behavior, with the nuclear spin affecting the electron spin time evolution, and the electron spin acting back on the dynamics of each of the nuclei in turn.

From the point of view of the electron spin, entanglement with the degrees of freedom of nuclear spins arising from the hyperfine coupling constitutes a decoherence mechanism.

Since the Overhauser field \mathbf{h} appearing in Eq. (51) is composed by the sum of a large number of spins, it is natural to question whether the nuclear field can be approximated to a classical object and to which extent this approximation gives correct results. In a relatively recent work by Coish *et al.* [23] it has been theoretically shown that, for the special case of a uniform hyperfine coupling constants $A_k = A/N$, arising from a constant wave function in the dot $\psi_0 = 1/\sqrt{v_0 N}$, the dynamics obtained in the mean field approximation and the quantum evolution show agreement up to the transverse-spin correlation time τ_c , which diverges in the zero external magnetic field case (unphysical result due to the assumption of constant coupling), but that saturates to a finite value in case of a finite external magnetic field.

1.10.2 Fluctuation timescales of the nuclear field. The nuclear field is quantum many-body interacting spin system whose field orientation and magnitude change over time. This change is due to the combined effect of the inter-nuclear dipole-dipole interaction and the hyperfine interaction between electron and the nuclei. The dipolar interaction does not conserve the total nuclear spin and thus can be responsible for changes in the nuclear spin configuration. Those changes, combined with the spatial variation of the hyperfine coupling constant, lead to a different value of the nuclear field seen by the electron spin and thus to its decoherence. Here we briefly outline the timescales in which those mechanisms take place, in order of decreasing timescales.

The strength of the effective magnetic dipole-dipole interaction between neighboring nuclei in GaAs is directly given by the width of the nuclear magnetic resonance (NMR) line to be $\sim (100\mu\text{s})^{-1}$ [24] and its inverse can be taken as an estimate for the timescale in which a change in the nuclear configuration due to dipolar interaction takes place, i.e. $T_{d-d} \approx 100\mu\text{s}$, which is just the period of precession of a nuclear spin in the local magnetic field generated by its neighbors. This timescale is so long that a great number of other decoherence mechanisms start to play a significant role before nuclear dipole effects start

to matter.

Besides spin diffusion driven by nuclear dipole-dipole interaction, the nuclear field can undergo a change due to the flip-flop term in the Hamiltonian Eq. (51). In a large external field B , the flip-flop term can be treated within the framework of perturbation theory, as it will be explained in the next section. We anticipate here that the hyperfine mediated dynamics in the nuclear field has a timescale given by $\propto A/N$. This means that up to this timescale the nuclear field can be considered as static.

1.11 *Decoherence due to hyperfine-induced electron spin dynamics*

An early treatment of the hyperfine interaction as a decoherence mechanism for single electron spins confined in quantum dots whose carried out in [22]. There, a second order time-dependent perturbation expansion of the hyperfine interaction in a magnetic field was performed with respect to the flip-flop transverse term $A(h_+S_- + h_-S_+)/2$ for a constant hyperfine coupling A and a long-time longitudinal spin-flip probability $\sim 1/p^2N$ is obtained, where p is the nuclear spin polarization. As a result beside a large external magnetic field, a large polarization p and a large number of nuclei in the dot would suppress the spin-flip probability.

The first signature of the non-Markovian behavior of the nuclear spin bath appeared in [26], where an exact solution for the fully polarized case $p = 1$ was provided. In that case the decoherence is due to a non-uniform hyperfine coupling that depends on the probability for the electron to be located at different nuclear sites. A remarkable feature of the non-Markovian behavior is the long-time power law decay of the electron spin correlator, $\sim 1/t^{3/2}$, in strong Zeeman field, according to which the longitudinal electron spin component decays of a fraction of $\sim 1/N$, in a time $\sim N/A$.

1.11.1 *Single-electron spin decoherence in large Zeeman splitting.* A detailed and comprehensive treatment of the hyperfine interaction [28] provides an analytical result for the electron spin dynamics for arbitrary nuclear spin I and nuclear polarization p . A generalized master equation (GME) approach allows a treatment of the transverse electron spin-nuclear spin flip-flop terms in the Hamiltonian with an external field in a well controlled perturbative way. An expansion of the self-energy in the exact Nakajima-Zwanzig GME shows a rich electron spin dynamics, with exponential and non exponential decaying contributions and undamped oscillations. The form of the decay of the transverse and longitudinal electron spin component is obtained in high magnetic field up to forth order in perturbation theory.

The hyperfine Hamiltonian in an external magnetic field is

$$\mathcal{H} = bS_z + \epsilon_{nz}I_z + \mathbf{h} \cdot \mathbf{S}, \quad (52)$$

where $b = g^* \mu_B B_z$ ($\epsilon_{nz} = g_I \mu_N B_z$) is the electron (nuclear) Zeeman splitting in a magnetic field defining the z -axis B_z , g^* (g_I) the effective electron (nuclear) g -factor, and μ_B (μ_N) the Bohr (nuclear) magneton. In the rotating frame with respect to the nuclear Zeeman term the Hamiltonian can be separated into a longitudinal (unperturbed) and transverse (perturbation) term,

$$\mathcal{H} = \underbrace{(b + h_z)S_z}_{\mathcal{H}_0} + \underbrace{(h_+ S_- + h_- S_+)/2}_V \quad (53)$$

In absence of V , $\langle S_z \rangle_t$ is constant, since $[\mathcal{H}_0, S_z] = 0$, but the transverse component $\langle S_{\pm} \rangle_t$ evolves in time in a non trivial way. For a large number of nuclear spins $N \sim 10^5$ (GaAs dot) a direct application of the central limit theorem gives a Gaussian distribution for the eigenvalues of h_z with mean $h_0 = \langle h_z \rangle$ and variance $\sigma \approx A/\sqrt{N}$. The transverse correlator for an initial state given by the product state of the initial electron spin state $\rho_S(0)$ and incoherent Gaussian distributed nuclear mixture state is

$$\langle S_{+} \rangle_t \approx \langle S_{+} \rangle_0 \exp[-t^2/2\tau^2 + i(b + h_0)t], \quad \tau = \frac{1}{\sigma} = \frac{2\hbar}{A} \sqrt{\frac{N}{1-p^2}}. \quad (54)$$

Choosing as nuclear initial state the pure state $|\psi_I(0)\rangle = \prod_j (\sqrt{1+p} |\uparrow_j\rangle + e^{i\phi_j} \sqrt{1-p} |\downarrow_j\rangle) / \sqrt{2}$, for a certain polarization p , the same result Eq. (54) with $h_0 = pN$ comes out.

The reason for this decay lies in the choice of the initial nuclear state containing many h_z eigenstates and can also be obtained choosing the nuclear field in a h_z eigenstate, but with the electron spin in a transverse initial state. This decay is reversible and can be removed with a standard spin echo technique [29,30]. Such an experiment therefore reveals only the decay due to the transverse flip-flop term V Eq. (52). A procedure more suitable for a quantum computation algorithm would be a strong Von Neumann measurement of the nuclear field that would then prepare a h_z eigenstate, leading to simple precession with no decay [31,32].

Analysis of the GME in the Born approximation for a very high magnetic field ($b \gg N$) provides an asymptotic form to leading orders in $\sim 1/\omega_n = 1/(b + h_n^z)$,

$$\langle S_{+} \rangle_t \approx \sigma_{+}^{\text{osc}}(t) + \sigma_{+}^{\text{dec}}(t), \quad \langle S_z \rangle_t \approx \langle S_z \rangle_{\infty} + \sigma_z^{\text{dec}}(t), \quad (55)$$

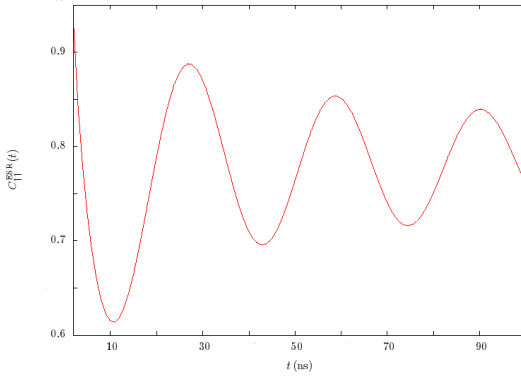


Figure 3. Decay of the driven Rabi oscillation in ESR showing a power law decay $\propto 1/\sqrt{t}$ and a universal phase shift of $\pi/4$, as given by Eq. (57), valid for $t \gg \max(1/\sigma, 1/b_{ac}, b_{ac}/2\sigma^2)$. For the plot the value $b = \sigma = 0.4$ Ghz have been chosen.

where $\langle S_z \rangle_\infty \propto \langle S_z \rangle_0$, $\sigma_+^{\text{osc}}(t) \propto \langle S_+ \rangle_0 e^{i\omega_n t}$, and $\sigma_{+/z}^{\text{dec}}(t) \propto \delta/t^{3/2}$ for a parabolic confinement in the dot, with $\delta \ll 1$. Even for a h_z eigenstate, for which no decay is expected in zeroth order in the transverse electron nuclear-spin flip-flop interaction, a long time irreversible decay takes place, that is due to the spatial variation of the hyperfine coupling constant.

1.11.2 Single-spin ESR: universal phase shift and power law decay. Here we describe the situation in which the electron spin is coherently driven via pulsed magnetic resonance, while coupled to a nuclear long-time correlated spin bath. Recent remarkable experimental results [30] show a coherent electron spin oscillation, even for a Rabi period much longer than $T_2^* = 10 - 20$ ns. A non-exponential decay of the Rabi oscillations is observed, obeying a power law decay with the appearance of a universal phase shift.

Consider a quantum dot in a time independent magnetic field defining the z direction. In addition, an oscillating magnetic field is applied in the plane, along the x direction. For a large number of nuclei in the dot ($N \sim 10^6$ in GaAs dots) the field h_z is Gaussian distributed, with mean h_0 and variance σ [25, 26, 28]. In the case of strong external field ($b \gg \sigma$, with $b = g^* \mu_B B_z$), neglecting transverse electron-nuclear spin flip-flop terms in the hyperfine interaction, the Hamiltonian is ($\hbar = 1$)

$$\mathcal{H} = (b + h_z)S_z + b_{ac} \cos(\omega t)S_x, \quad (56)$$

where $b_{ac} = g^* \mu_B B_{ac}$, ω and B_{ac} being the frequency and amplitude of the ESR driving field. h_z is considered static (justified for $t < 1\mu\text{s}$), and the assumption $\omega = b + h_0$ is made. In the rotating wave approximation (valid for

$(b_{\text{ac}}/b)^2 \ll 1$), after averaging over the Gaussian distribution of h_z , the decay of the driven Rabi oscillation is given by [30]

$$P_{\uparrow}^{\text{ESR}}(t) \sim 1 - C + \sqrt{\frac{b_{\text{ac}}}{8\sigma^2 t}} \cos\left(\frac{b_{\text{ac}}}{2}t + \frac{\pi}{4}\right) + \mathcal{O}\left(\frac{1}{t^{3/2}}\right), \quad (57)$$

for $t \gg \max(1/\sigma, 1/b_{\text{ac}}, b_{\text{ac}}/2\sigma^2)$, with $C = \exp(b_{\text{ac}}^2/8\sigma^2) \text{erfc}(b_{\text{ac}}/\sqrt{8}\sigma) \sqrt{2\pi} b_{\text{ac}}/8\sigma$. The remarkable features appearing in the experiment are the $\sim 1/\sqrt{t}$ power law decay and the universal $\pi/4$ phase shift. The reason for the appearance of these features is that the nuclear field h_z does not change over a timescale much longer than the Rabi period. Since different values of h_z determine different oscillation frequencies, an average over the distribution in h_z give rise to a decay in the coherence of the driven electron spin, and the off-resonant contributions also determine the phase shift. The fact that coherent Rabi oscillations are visible even when the Rabi period is much longer than the transverse spin decay time $\tau \sim 15\text{ns}$ has its origin in the fact that the power law decay sets in already after a short time $1/\sigma \sim 15\text{ns}$.

In order to measure the electron spin state in the experiment [30], a spin-charge conversion technique is implemented by operating a double quantum dot in the spin blockade regime [33, 34], in which the transport through the dots can occur only via transitions from spin states with one electron per dot, $|(1, 1)\rangle$, to the singlet state in the right dot, $|(0, 2)\rangle$. The Pauli exclusion principle, that does not allows two electron with same spin state to occupy the same orbital, allows transport only for antiparallel spins. Transport of states spin-triplet states is therefore blocked. The oscillating transverse magnetic field rotates the spins, therefore unblocking an initial state with even parity spin state [34].

1.11.3 Single-triplet decoherence in a double quantum dot. An alternative way to implement a qubit with electron spin in quantum dots is to consider a double quantum dot with two spins, one per dot, and encode the qubit in the subspace with zero z -projection of the total spin $S_{\text{tot}}^z = S_1^z + S_2^z = 0$. Advantages of this scheme is the possibility of reducing the hyperfine coupling in case of symmetric dots. At the same time additional decoherence due to the coupling to the orbital degree of freedom and leakage errors may appear.

The effective Hamiltonian for the one-electron-per-dot configuration can be written as

$$\mathcal{H}_{dd} = \epsilon_z S_z + \mathbf{h} \cdot \mathbf{S} + \delta \mathbf{h} \cdot \delta \mathbf{S} + \frac{J}{2} \mathbf{S} \cdot \mathbf{S} - J, \quad (58)$$

where $\mathbf{S} = \mathbf{S}_1 + \mathbf{S}_2$, $\delta\mathbf{S} = \mathbf{S}_1 - \mathbf{S}_2$, $\mathbf{h} = \mathbf{h}_1 + \mathbf{h}_2$, and $\delta\mathbf{h} = \mathbf{h}_1 - \mathbf{h}_2$. Here J is the Heisenberg exchange coupling between the two electron spins. For definiteness we work in a regime of large Zeeman splitting due to an external magnetic field, $\epsilon_z = g^* \mu_B \gg \max\{\langle\delta\mathbf{h}\rangle_{\text{rms}}, \langle\mathbf{h}\rangle_{\text{rms}}\}$, where $\langle\mathcal{O}\rangle_{\text{rms}} = \langle\psi_I|\mathcal{O}|\psi_I\rangle^{1/2}$ denotes the root-mean-square expectation value of the operator \mathcal{O} on the nuclear state $|\psi_I\rangle$. Requiring $\epsilon_z \gg J$, where J is taken to be positive without loss of generality, the large Zeeman splitting condition renders the relevant spin Hamiltonian block diagonal with respect to the eigensubspaces of S_z . In the $S_z = 0$ subspace the spin Hamiltonian for the singlet $|S\rangle$ and $S_z = 0$ triplet $|T_0\rangle$, to zeroth order in the inverse Zeeman splitting $1/\epsilon_z$, is given by $\mathcal{H}_0 = (J/2)\mathbf{S} \cdot \mathbf{S} + \delta h^z \delta S^z$. The effective qubit Hamiltonian in terms of the vector consisting of Pauli matrices $\boldsymbol{\tau} = (\tau^x, \tau^y, \tau^z)$, with the computational states $|S\rangle \rightarrow |\tau^z = -1\rangle$ and $|T_0\rangle \rightarrow |\tau^z = 1\rangle$, has the form

$$\mathcal{H}_0 = \frac{J}{2}(1 + \tau^z) + \delta h^z \tau^x. \quad (59)$$

A systematic treatment of the dynamics induced by the Hamiltonian Eq. (59) can be found in [31, 35]. The eigenstates of \mathcal{H}_0 are given by a product state between a nuclear eigenstate $|n\rangle$ of δh^z and a superposition of $|S\rangle$ and $|T_0\rangle$, therefore \mathcal{H}_0 does not lead to any dynamics in the nuclear field. The correlator C_{T_0S} is defined as the probability to find the electron spins in the state $|T_0\rangle$ at time $t > 0$, provided the initial state ($t = 0$) was $|\psi(0)\rangle = |S\rangle \otimes |\psi_I\rangle$, with $|\psi_I\rangle$ a superposition of δh^z eigenstates,

$$C_{T_0S}(t) = \sum_n \rho_I(n) |\langle n| \otimes \langle T_0| e^{-i\mathcal{H}_0 t} |S\rangle \otimes |n\rangle|^2, \quad (60)$$

where $\rho_I(n)$ diagonal matrix element of $|\psi_I\rangle\langle\psi_I|$ in the $\{|n\rangle\}$ basis. For a Gaussian distributed field δh_z , with mean x_0 and variance σ_0 , the asymptotics of C_{T_0S} saturates to finite value that deviates from the semiclassical results [$C_{T_0S}^{\text{semicl}}(\infty) = 1/2$] for $J \ll x_0$ [35]

$$C_{T_0S}(\infty) \sim \begin{cases} \frac{1}{2} - \frac{1}{8} \left(\frac{J}{x_0}\right)^2, & \sigma_0, J \ll x_0, \\ 2 \left(\frac{x_0}{J}\right)^2, & \sigma_0 \ll x_0 \ll J. \end{cases} \quad (61)$$

At short times $C_{T_0S}(t)$ experiences a Gaussian decay on a timescale $\sqrt{J^2 + 4x_0^2}/4x_0\sigma_0$, while in the case of strong coupling $J \gg \max\{x_0, \sigma_0\}$

at long times $t \gg J/4\sigma_0^2$ a power law decay appears, [35]

$$C_{T_0S}(t) \sim C_{T_0S}(\infty) - \frac{e^{-x_0^2/2\sigma_0^2}}{4\sigma_0\sqrt{Jt}} \cos\left(Jt + \frac{3\pi}{4}\right). \quad (62)$$

Those results show that the singlet-triplet correlator decays due to the quantum distribution of the nuclear spin system, even for a static system. For non zero exchange interaction $J \neq 0$ the asymptotic behavior of the correlator $C_{T_0S}(t)$ changes from a short time Gaussian behavior to a long time power-law ($\sim 1/t^{3/2}$) decay and acquires a universal phase shift which is $3\pi/2$, consistent with experimental findings for the correlator $C_{SS}(t)$ [36]. Qualitatively similar results appear when looking at the transverse correlator in the $S_z = 0$ subspace, though one finds different decay power and different value of the universal phase shift.

1.12 Nuclear spin state manipulation

As mentioned in the previous sections, for a system of N unpolarized nuclei and an effective hyperfine interaction strength A , the dephasing time in a weak magnetic field is $T_2^* \sim 1/\sigma \sim \sqrt{N}/A$, where σ is the width of the distribution of the nuclear field h_z . This decay T_2^* finds its origin in the ensemble average over the field distribution. In order to prolong the electron spin coherence, narrowing of the nuclear field distribution was proposed in [28] as an alternative to the strategy of polarizing the nuclear spins [22], that would require a polarization close to 100% to be efficient, which is currently not available [28]. Few methods for nuclear spin state narrowing have been studied, in Ref. [31] the narrowing is due to gate-controlled Rabi oscillations in a double quantum dot in which the exchange interaction oscillates, in Ref. [37] a scheme based on quantum phase estimation is envisioned for a single undriven spin in a single quantum dot, and in Ref. [32] the narrowing is achieved by optical preparation.

1.12.1 Nuclear state narrowing by qubit state measurement. Here we discuss a nuclear state narrowing technique that has been proposed in [31]. Consider for definiteness the ESR Hamiltonian Eq. (56). The effective Zeeman splitting is given by $b + h_z^n$, where $b = g^*\mu_B B_z$ and h_z^n is an eigenvalue of h_z . The idea behind state narrowing is that the ESR driving give rise to the resonance condition $b + h_z^n - \omega = 0$, such that the evolution of the electron spin depends on the nuclear spin state and thus a determination of the electron spin evolution results in a determination of the nuclear spin state.

The eigenvalues of the nuclear field, as already mentioned in the previous sections, are Gaussian distributed in equilibrium. The diagonal elements of

the nuclear spin density matrix are $\rho_I(h_z^n, t=0) = \langle h_z^n | \rho_I | h_z^n \rangle = \exp(-(\hbar_z^n - \langle h_z \rangle)^2 / 2\sigma^2) / \sqrt{2\pi}\sigma$, with mean $\langle h_z \rangle$ and variance σ . Therefore, initializing the electron spin in the state $|\uparrow\rangle$ at time $t=0$, the probability to find the electron spin in the state $|\downarrow\rangle$ is given by

$$P_{\downarrow}(t) = \int dh_z^n \rho_i(h_z^n, 0) P_{\downarrow}^n(t), \quad (63)$$

where $P_{\downarrow}^n(t)$ is the probability to find the electron spin in the state $|\downarrow\rangle$, for a given an eigenvalue h_z^n of the nuclear field h_z ,

$$\begin{aligned} P_{\downarrow}^n(t) &= |\langle h_z^n | \otimes \langle \downarrow | U^{\text{ESR}}(t) | \uparrow \rangle \otimes | h_z^n \rangle|^2 \\ &= \frac{1}{2} \frac{b_{\text{ac}}^2}{b_{\text{ac}}^2 + 4\delta_n^2} \left[1 - \cos \left(\frac{t}{2} \sqrt{b_{\text{ac}}^2 + 4\delta_n^2} \right) \right]. \end{aligned} \quad (64)$$

If at time $t = t_m$ we perform a measurement of the electron spin and find $|\downarrow\rangle$, the diagonal element of the nuclear spin density matrix will change according to

$$\rho_I(h_z^n, 0) \rightarrow \rho_I^{(1,\downarrow)}(h_z^n, t_m) = \rho_I(h_z^n, 0) \frac{P_{\downarrow}^n(t_m)}{P_{\downarrow}(t_m)}. \quad (65)$$

In the case where a measurement is performed with a low time resolution Δt , $\Delta t \gg 1/b$, such that it gives the time averaged value, the probability turns out to be $P_{\downarrow}^n = \lim_{T \rightarrow \infty} (1/T) \int_0^T dt P_{\downarrow}^n(t) = b_{\text{ac}}^2 / 2(b_{\text{ac}}^2 + 4\delta_n^2)$. Therefore, a measurement on the electron spin with outcome $|\downarrow\rangle$ results in a multiplication of the nuclear spin density matrix by a Lorentzian, with width b_{ac} , centered around the h_z^n that satisfied the condition $b + h_z^n - \omega = 0$. The nuclear spin distribution, thus, undergoes a narrowing, resulting in an enhancement of the electron spin coherence, if $b_{\text{ac}} < \sigma$. In the case that the measurement outcome is $|\uparrow\rangle$ the diagonal element of the nuclear spin density matrix will change according to

$$\rho_I(h_z^n, 0) \rightarrow \rho_I^{(1,\uparrow)}(h_z^n, t_m) = \rho_I(h_z^n, 0) \frac{1 - P_{\downarrow}^n(t_m)}{1 - P_{\downarrow}(t_m)}, \quad (66)$$

resulting in a reduced probability for the nuclear field to have a value that matches the resonance condition $b + h_z^n - \omega = 0$.

This procedure can be iterated many times before changes due to the slow internal dynamics start to affect the nuclear spin state. Many measurement of the electron spin are possible within this time, with re-initialization of the

electron spin state between the measurements. Assuming that M cycles can be performed with a static nuclear field, we have

$$\rho_I(h_z^n, 0) \rightarrow \rho_I^{(M, \alpha_\uparrow)}(h_z^n, t_m) = \frac{1}{N} \rho_I(h_z^n, 0) (P_\downarrow^n)^{\alpha_\uparrow} (1 - P_\downarrow^n)^{M - \alpha_\uparrow}, \quad (67)$$

where α_\uparrow is the number of measurement outcomes $|\downarrow\rangle$. If the outcome is $|\downarrow\rangle$ the narrowing has been achieved, otherwise, it is necessary to wait for a re-equilibration of the nuclear system before the next measurement.

1.12.2 Optical preparation of nuclear spins. Here we discuss the case of optical nuclear spin preparation that makes use of spin-flip two-photon Raman resonance in a driven three-level system (TLS) [32]. The lowest electronic states in GaAs quantum dots that are optically active under σ_+ circularly polarized excitation are the ground state of a single localized conduction-band (E_C) electron, in which a Zeeman field splits the up and down spin states, and the negatively charged exciton (trion) $|X\rangle$, given by two electrons with antiparallel spin plus one valence band heavy hole (hh) with angular momentum $J_{z'} = +3/2$, as schematically shown in Fig. 4. The $J = 3/2$ subspace in the valence band split up into heavy and light holes (hh and lh) along the direction z' of strong quantum dot confinement, that is in general different from the z -axis in the conduction band, chosen to be the direction of the magnetic field B . The two circularly polarized lasers stimulate the transition between $|\uparrow\rangle$ and $|X\rangle$ at frequency $\omega_p = \omega_X - \omega_\uparrow - \Delta_1$ and the transition between $|\downarrow\rangle$ and $|X\rangle$ at frequency $\omega_c = \omega_X - \omega_\downarrow - \Delta_2$, while the trion $J_{z'} = -3/2$ is not excited.

The narrowing of the nuclear field distribution is based on light scattering in the TLS, where two long-lived spin states are resonantly coupled to the excited trion state $|X\rangle$ that decays spontaneously. For the two-photon resonance condition $\delta = \Delta_1 - \Delta_2 = 0$, where δ is the detuning of the difference of the frequency of the two lasers $\omega_c - \omega_p$ from the Zeeman splitting ω_z of the two spin states, the system is in a superposition of the two spin states with a vanishing excited state component, and the system is driven to a dark state with no photon emission. In presence of a nuclear spin field, the resonance moves to $\delta = \delta h_z$, where δh_z is the deviation of the Overhauser field from its mean. Monitoring the photon emission constitutes a continuous weak measurement of the Overhauser field h_z . The absence of photon emission in the limit $t \rightarrow \infty$, corresponding to the strong measurement limit, would project the nuclear state onto $|\delta h_z = 0\rangle$, with width $\sigma = 0$, therefore letting the dephasing time to diverge, $T_2^* \sim 1/\sigma \rightarrow \infty$. A continuous weak measurement of the Overhauser field, supported by an adaptive adjustment of the lasers frequencies every time a photon is detected, leads to a narrowing of the nuclear

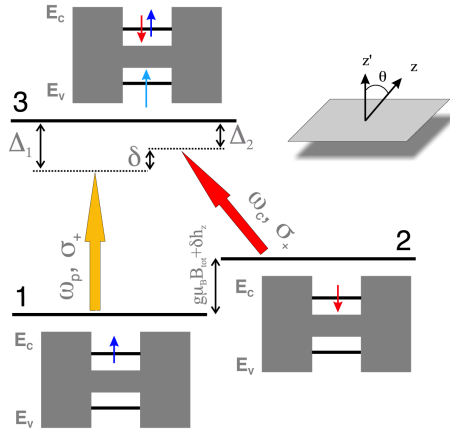


Figure 4. Three-level system. The states 1(2) are spin-up (-down) conduction-band (E_C) electron, with splitting given by $g\mu_B B_{\text{tot}} + \delta h_z$, where δh_z is the z component of the nuclear field fluctuations. State 3 is a trion with $J_{z'} = 3/2$ (With permission from the Authors).

field distribution, and an enhancement of the phase coherence of the electron spin.

The relevant effective Hamiltonian of the TLS in the rotating wave approximation is block diagonal, with blocks labeled by the eigenvalues δh_z^k of the field δh_z

$$\mathcal{H}_k = -\frac{\hbar}{2} \begin{pmatrix} \delta h_z^k + \delta & 0 & \Omega_p \\ 0 & -\delta h_z^k - \delta & \Omega_c \\ \Omega_p & \Omega_c & -\Delta \end{pmatrix}, \quad (68)$$

where $\Delta = \Delta_1 + \Delta_2$. The combined system consisting of the TLS and the nuclear spins evolves in time according to a generalized master equation $\dot{\rho} = \mathcal{L}\rho$, where \mathcal{L} is the Liouvillian operator defined as

$$\dot{\rho} = \mathcal{L}\rho \equiv \frac{1}{i\hbar} [H, \rho] + \mathcal{W}\rho, \quad (69)$$

where H is the Hamiltonian of the system, and $\mathcal{W} = \sum_{\alpha=\uparrow,\downarrow} \Gamma_{X\alpha} (2\sigma_{\alpha X} \rho \sigma_{X\alpha} - \sigma_{XX} \rho - \rho \sigma_{XX})/2 + \sum_{\beta=\uparrow,\downarrow} \gamma_{\beta} (2\sigma_{\beta\beta} \rho \sigma_{\beta\beta} - \sigma_{\beta\beta} \rho - \rho \sigma_{\beta\beta})/2$. Here the rate $\Gamma_{X\alpha}$ describes the radiative decay of $|X\rangle$ into $\alpha = |\uparrow\rangle, |\downarrow\rangle$, while γ_{β} is the pure dephasing rate of state $\beta = |\downarrow\rangle, |X\rangle$ with respect to $|\uparrow\rangle$.

Taking as initial state a product of arbitrary density matrices χ_0 for the TLS and $\nu_0 = \sum_{kk'} \nu_{kk'} |\delta h_z^k\rangle \langle h_z^{k'}|$ for the nuclear field, the stationary solution is an entangled state $\bar{\rho}$.

In order to describe the state of the system conditional on a measurement

record, a conditional density matrix is used. The *a posteriori* distribution ν_{kk} is found to be concentrated around the two photon resonance. The stationary emission rate is

$$\Gamma_{\text{em}} = \text{Tr} \mathcal{S} \bar{\rho}(t) = \Gamma \sum_k \nu_{kk} \langle X | \rho_{kk} | X \rangle, \quad (70)$$

where $\Gamma = \Gamma_{X\uparrow} + \Gamma_{X\downarrow}$ and \mathcal{S} is the collapse operator, describing spontaneous emission of the state $|X\rangle$ into $|\uparrow\rangle$ and $|\downarrow\rangle$ at rates $\Gamma_{X\uparrow}$ and $\Gamma_{X\downarrow}$. the update rule for ν upon photon emission is

$$\nu'_{kk} = \frac{\nu_{kk} \langle X | \rho_{kk} | X \rangle}{\sum_j \nu_{jj} \langle X | \rho_{jj} | X \rangle}. \quad (71)$$

The population in the Overhauser field δh_z corresponding to the two-photon resonance $\delta h_z = \delta$ is depleted by the photon emission. The electron spin coherence is quantified by the time dependence of the transverse electron spin component, which in turn is given by the Fourier transform of the nuclear field distribution, $\langle S_+(t) \rangle = (\hbar/2) \sum_k \nu_{kk} \exp(it\delta h_z^k)$. The repeated observation of the quantum dot photon emission and consequent adaption of the laser frequencies after each photon detection leads to a narrowing in the nuclear distribution and consequent enhancement of the electron spin coherence time.

1.12.3 Exponential decay in narrowed nuclear state. We have seen that the nuclear spin bath induces a non-Markovian dynamics of the electron spin, with super-exponential or power-law decay of the correlation functions. On the other hand it has been argued that a narrowing of the nuclear spin distribution is expected to prolong the electron spin coherence. In [38] it is shown that, in case of a large Zeeman splitting and for a particular narrowed nuclear spin state, a Markovian dynamics can arise from virtual flip-flops between the electron spin and the nuclear spin system, with simple exponential decay.

The Hamiltonian describing the interaction of the electron spin with the nuclear system in a large magnetic field is given by Eq. (53). The energy non-conserving term V can be eliminated by means of a Schrieffer-Wolff transformation, $\tilde{\mathcal{H}} = e^S \mathcal{H} e^{-S} \approx H = \mathcal{H}_0 + \frac{1}{2}[S, V]$, where $S = \mathcal{L}_0 V$, and \mathcal{L}_0 is the unperturbed Liouvillian, defined by $\mathcal{L}_0 O = [\mathcal{H}_0, O]$. The effective Hamiltonian H is given by

$$H = (\omega + X)S^z + D. \quad (72)$$

The operators ω , D and X are nuclear spin operators and the first two are diagonal in a product-state basis of I_k^z -eigenstates, whereas X is purely off-

diagonal and produces correlations between nuclear spins. Corrections of the order of $\sim A^2/Nb$ in the diagonal terms of H are neglected, whereas the term of this size in X are retained. This assumption is valid as long as the bath correlation time τ_c is much shorter than the time scale after which the diagonal corrections become relevant for $b \gg A$, where a Born-Markov approximation is valid: $\tau_c \sim N/A \ll Nb/A^2$. As a result $\omega = b + h^z$.

The electron and nuclear states are assumed to be initially unentangled and the nuclear system is prepared in a narrowed state, $\omega|n\rangle = \omega_n|n\rangle$. For this initial conditions, the dynamics of the transverse electron spin component $\langle S_+ \rangle_t$ is described by a GME, and can be written in a rotating frame defined by $x_t = \exp[-i(\omega_n + \Delta\omega)t] \langle S_+ \rangle_t$, where $\Delta\omega$ is a frequency shift self-consistently defined by $\Delta\omega = -\text{Re} \int_0^\infty dt \Sigma(t)$, with $\tilde{\Sigma}(t) = \exp[-i(\omega_n + \Delta\omega)t] \Sigma(t)$, through the memory kernel $\Sigma(t)$ of the GME. The equation of motion for x_t is given by

$$\dot{x}_t = -i \int_0^t d\tau \tilde{\Sigma}(\tau) x_{t-\tau}. \quad (73)$$

If $\Sigma(t)$ decays to zero sufficiently fast on the time scale $\tau_c \ll T_2$, where T_2 is in turn the decay time of x_t , it is possible to approximate $x_{t-\tau} \approx x_t$ and extend the upper limit of the integral to infinity, $t \rightarrow \infty$, obtaining a Markovian dynamics

$$x_t = \exp(-t/T_2) x_0 + \epsilon(t), \quad \frac{1}{T_2} = -\text{Im} \int_0^\infty dt \tilde{\Sigma}(t), \quad (74)$$

where $\epsilon(t)$ gives a small non-Markovian correction that can be bounded precisely if $\tilde{\Sigma}(t)$ is known.

For a homo nuclear system, by expanding $\Sigma(t)$ in the perturbation $V = X S^z$ and retaining only leading orders in the Born approximation in the small parameter A/ω_n , the decoherence time T_2 can be cast in the compact form

$$\frac{1}{T_2} = \text{Re} \int_0^\infty dt e^{-i\Delta\omega t} \langle X(t) X \rangle, \quad X(t) = e^{-i\omega t} X e^{i\omega t}, \quad (75)$$

where the average stands for an expectation value taken with respect to the initial nuclear state. Though the compact form resembles the standard result for pure dephasing valid in a weak coupling expansion, here there is no such weak coupling expansion. The decoherence rate $1/T_2$ depends on the correlator $C(t) = \langle X(t) X \rangle$. For an isotropic electron wave function of the form $\psi(r) = \psi(0) e^{-(r/r_0)^{d/2}}$ containing $N \gg 1$ nuclei within a radius r_0 in d dimension, the asymptotic dependence of $C(t)$ at long times is $C(t) \propto 1/t^{2d/q}$, for $t \gg N/A$

and $d/q < 2$. For $d/q \leq 1/2$, $1/T_2$ given by Eq. (75) diverges and no Markov approximation is valid within the Born approximation. On the other hand, for a 2D dot with a Gaussian electron wave function and for unpolarized nuclear system, Eq. (75) gives the simple result

$$\frac{1}{T_2} = \frac{\pi}{3} \left(\frac{I(I+1)A}{3b} \right)^2 \frac{A}{N}. \quad (76)$$

The condition for the validity of the the Markov approximation, $T_2 > \tau_c \sim N/A$ is satisfied whenever $A/b < 1$, which correspond to the range of validity of the Born approximation. Remarkably, from last equation it follows that $1/T_2$ strongly depends on the magnitude of the nuclear spin, $1/T_2 \propto I^4$. Therefore, systems with large nuclear spin, such as In ($I_{\text{In}} = 9/2$), will show faster decay.

With these last results on exponential decay in a spin bath, we conclude the part on electron spin decoherence induced by the nuclear spin system and focus on phonon-mediated relaxation of the electron spin in quantum dots.

1.13 Phonon-induced relaxation in quantum dots

Electron spin relaxation in quantum dots takes place via transitions between spin states, with consequent energy dissipation in the environment. In a quantum dot the dissipative environment is represented mainly by the phonons in the surrounding crystal. Therefore, in order to fully understand relaxation and decoherence mechanisms that occur in quantum dots, it is important to understand the manner in which the electron spin interacts with phonons.

Spin-orbit interaction creates an admixture of orbital and spin degrees of freedom of the electron, and represents an effective coupling mechanism that mediates the spin-phonon interaction, and that, ultimately, is responsible for relaxation of the electron spin. Phonons can produce electric field fluctuations that can lead to spin relaxation of eigenstates of the spin-orbit Hamiltonian. Two kinds of electron-phonon interactions are taken into account, that arise, respectively, from an inhomogeneous deformation of the crystal potential, resulting in an alteration of the band-gap, and a homogeneous strain due to piezo-electric effect, the former taking place in all semiconductors, the latter only in crystals without structure inversion symmetry such as GaAs.

1.14 Introduction: Spin-orbit interaction

An electron that moves in an electric field experiences an effective magnetic field in its rest frame which interacts with the spin of the electron. The internal magnetic field depends on the orbital the electron occupies and therefore spin

and orbit are coupled. This well known effect comes directly from the relativistic Dirac theory of point particles and it goes under the name of spin-orbit (SO) interaction. The SO Hamiltonian has the general form [39]

$$\mathcal{H}_{\text{SO}} = \frac{\hbar}{4m_0^2c^2} \mathbf{P} \cdot (\boldsymbol{\sigma} \times \nabla V), \quad (77)$$

where m_0 is the free electron mass, c is the speed of light, $\boldsymbol{\sigma} = (\sigma_x, \sigma_y, \sigma_z)$ is the Pauli matrix vector, and V is the electric potential. In presence of an external magnetic field $\mathbf{B} = \nabla \times \mathbf{A}$, the canonical momentum \mathbf{p} is replaced by the kinetic momentum $\mathbf{P} = \mathbf{p} + e\mathbf{A}$, \mathbf{A} being the vector potential.

In semiconductors like Si or Ge the crystal lattice has spatial inversion symmetry. For such materials, states of a given momentum \mathbf{k} are 4-fold degenerate at $B = 0$. In fact due to time reversal symmetry, $\epsilon_{\mathbf{k},\uparrow} = \epsilon_{-\mathbf{k},\downarrow}$ holds, and from the inversion symmetry one has $\epsilon_{\mathbf{k},\sigma} = \epsilon_{-\mathbf{k},\sigma}$, such that $\epsilon_{\mathbf{k},\uparrow} = \epsilon_{\mathbf{k},\downarrow}$ holds.

The double degeneracy can be broken either via the application of an external magnetic field, which breaks the time reversal symmetry, or via the break of spatial inversion symmetry. This is indeed what happens in crystals that exhibit bulk inversion asymmetry (BIA), such as the zincblende structure of GaAs. This effect is known as Dresselhaus spin-orbit interaction [40, 41]. The Hamiltonian for 2D systems results from the 3D bulk Hamiltonian [42] after integration over the growth direction z along [001]

$$\mathcal{H}_D \propto [-\sigma_x p_x \langle p_z^2 \rangle + \sigma_y p_y \langle p_z^2 \rangle + \sigma_x p_x p_y^2 - \sigma_y p_y p_x^2] \quad (78)$$

where x and y point along the crystallographic directions [100] and [010]. Due to the strong confinement along z , the terms cubic in momentum components appearing in the Hamiltonian are usually much smaller than the linear ones, and they are usually neglected. Retaining only the linear term

$$\mathcal{H}_D = \beta(-\sigma_x p_x + \sigma_y p_y) \quad (79)$$

where β depends on material properties and on $\langle p_z^2 \rangle$. The spin dynamics resulting from the Dresselhaus Hamiltonian is well understood in the case of circular orbit, in which the spin rotates in the opposite direction with respect to the orbit, as shown in Fig. 5.

In heterostructures like GaAs/AlGaAs, an asymmetric confining potential additionally breaks the inversion symmetry, giving rise a further spin-orbit interaction due to structural inversion asymmetry (SIA), known as Bychkov-Rashba term [43, 44]. For a confining electric field along the z direction, the

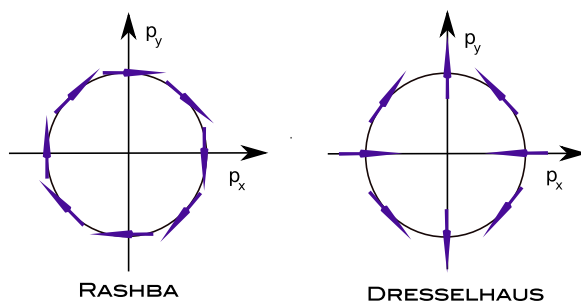


Figure 5. Schematic representation the apparent momentum dependent field $\Omega(\mathbf{p})$ in the spin-orbit Hamiltonian, $\Omega(\mathbf{p}) \cdot \sigma$, for the Dresselhaus and Rashba spin-orbit interactions.

Bychkov-Rashba Hamiltonian $\propto (\mathbf{E} \times \mathbf{p}) \cdot \sigma$ is

$$\mathcal{H}_R = \alpha(\sigma_x p_y - \sigma_y p_x), \quad (80)$$

where α depends on the confining potential and on material properties. The spin dynamics resulting from the Bychkov-Rashba Hamiltonian can also be well understood in the case of circular orbit, in which the spin rotates along in the same direction as the orbit, being the spin always antiparallel to the direction of motion, as explained in Fig. 5.

1.15 Electron spin relaxation and decoherence

Due to the fact that the most promising semiconductor devices that make use of the electron spin as the quantum two level system (qubit) are realized on the basis of 2D electron gases in GaAs heterostructures, the following discussion concentrates on spin flip mechanisms that are relevant for GaAs.

Spin relaxation of localized electrons in quantum dots shows remarkable differences from the case of delocalized bulk electrons. The most effective mechanisms in bulk 2D are related to the broken inversion symmetry, either the BIA or SIA case, which give rise to a strong spin-orbit splitting in the electron spectrum, ultimately responsible for spin flip. Besides, the piezoelectric interaction arising in non-inversion symmetric crystals provides a strong coupling of electrons to the bosonic bath of acoustic phonons. The interplay of these mechanisms results in an efficient spin-lattice relaxation for bulk carriers in III-V type semiconductors and heterostructures. The strong localization of electrons in quantum dots leads to suppression of spin-flip rate. The phonon-assisted spin-flip mechanisms in semiconductor quantum dots have been studied in [18, 19].

1.15.1 Electron spin relaxation in quantum dots. In the case of strong confinement in the z direction, corresponding to the [100] crystallographic axis, for a lateral dot size much larger than the degree of vertical confinement, the Hamiltonian derived from the Kane model [45] for 2D electrons in the conduction band in the presence of an external magnetic field \mathbf{B} is [18, 19]

$$\mathcal{H} = \frac{\mathbf{p}^2}{2m} + U(\mathbf{r}) + U_{\text{ph}}(\mathbf{r}, t) + \frac{1}{2}g\mu_B\boldsymbol{\sigma} \cdot \mathbf{B} + \mathcal{H}_{SO}^D + \mathcal{H}_{SO}^R, \quad (81)$$

$$\mathcal{H}_{SO}^D = \beta(-\sigma_x p_x + \sigma_y p_y), \quad \mathcal{H}_{SO}^R = \alpha(\sigma_x p_y - \sigma_y p_x). \quad (82)$$

Here $\mathbf{p} = -i\hbar\nabla + (e/c)\mathbf{A}$ is the kinetic momentum, m the effective mass, g the effective electron g -factor (in GaAs $g = -0.44$), and $\boldsymbol{\sigma}$ the Pauli matrix vector. The axes x , y , and z coincide with the main crystallographic ones, with z perpendicular to the 2D plane. The first two terms of the Hamiltonian describe the quantum dot with confining potential $U(\mathbf{r})$, that is typically chosen parabolic. The third term describes the spin-independent interaction with acoustic phonon. The fourth term is the Zeeman Hamiltonian. \mathcal{H}_{SO} describes the spin-orbit effects. \mathcal{H}_{SO}^D is the Dresselhaus term, due to BIA, and \mathcal{H}_{SO}^R is the Rashba term, due to SIA. For GaAs heterostructures $\beta \approx 10^5$ cm/s.

The Hamiltonian of Eq. (81) should contain also term describing “direct” interaction between spin and phonons, such as that due to an inhomogeneous deformation of the lattice, and a term describing the spin-phonon coupling in presence of a magnetic field due to a lattice-deformation-dependent admixture of valence-band and conduction-band states. Their contribution on spin relaxation rates turns out to be negligible with respect to the dominant admixture mechanism contribution ascribable to the Dresselhaus and Rashba spin-orbit interaction. See Ref. [18, 19, 46] for a discussion of the direct spin-phonon coupling contribution.

The phonon-induced rate for the transition between $|\Psi_n^\uparrow\rangle$ and $|\Psi_n^\downarrow\rangle$ is given by Fermi’s golden rule

$$\Gamma = \frac{2\pi}{\hbar} \sum_n |\langle \Psi_n^\uparrow | \mathcal{H}_{ph} | \Psi_n^\downarrow \rangle|^2 D(\epsilon_z). \quad (83)$$

Here $D(E)$ is the phonon density of states at the Zeeman energy splitting ϵ_z . From experimental results, the relevant acoustic phonons can be treated as bulk-like phonons, showing a linear dispersion relation in the relevant energy range, for which the density of states increases quadratically with energy [20]. The states $|\Psi_n^\uparrow\rangle$ and $|\Psi_n^\downarrow\rangle$ are the effective spin states, containing more than one orbital and both the spin *up* and *down* states. This admixture of spin and orbit comes out in taking into account the spin-orbit interaction due to BIA

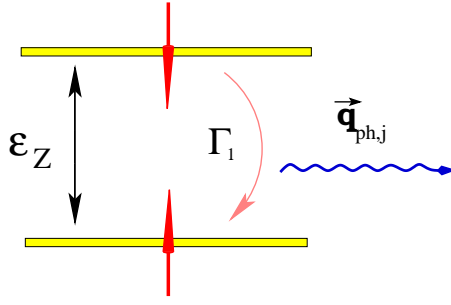


Figure 6. Schematic representation of the spin-flip process associated with the emission of a phonon of energy ϵ_Z and momentum \mathbf{q}_j , where j is the branch index, at rate Γ_1 .

and SIA as a perturbation. Due to the localization of stationary states in a quantum dot, it follows that the spin-orbit interaction does not directly couple Zeeman-split sublevels in the same quantum dot orbital. It follows that within first order perturbation theory in the spin-orbit Hamiltonian, the effective single electron quantum dot states are

$$|\Psi_n^\uparrow\rangle = |n \uparrow\rangle + \sum_{n' \neq n} \frac{(\mathcal{H}_{SO})_{n'n}^{\downarrow\uparrow}}{E_n - E_{n'} + g\mu_B B} |n' \downarrow\rangle, \quad (84)$$

$$|\Psi_n^\downarrow\rangle = |n \downarrow\rangle + \sum_{n' \neq n} \frac{(\mathcal{H}_{SO})_{n'n}^{\uparrow\downarrow}}{E_n - E_{n'} - g\mu_B B} |n' \uparrow\rangle, \quad (85)$$

where $(\mathcal{H}_{SO})_{n'n}^{\downarrow\uparrow} = \langle n' \downarrow | \mathcal{H}_{SO} | n \uparrow \rangle$ and $\{|n\rangle\}$ are the unperturbed quantum dot orbital states. Due to the anisotropy of BIA and SIA spin-orbit interaction, the admixture of spin and orbit degrees of freedom turns out to be anisotropic [47].

For spin-flip transitions involving a small energy transfer, the dominant contribution comes from piezo-electric phonons. The electric field associated with a single phonon scales like $1/\sqrt{q}$ for piezo-phonons and like \sqrt{q} for deformation potential phonons, q being the phonon wave number. This is due to the fact that piezo-phonons come from a homogeneous lattice strain, in which long wavelengths play a major role. Vice versa, a local deformation would involve short wavelengths, and so higher energies. On the other hand, wavelengths much longer than the dot size give rise to a global shift of the entire dot potential, therefore the effective phonon wavelengths are those comparable with the dot size, as seen in [48].

The electron-phonon coupling for piezo-electric phonons has the form

$$U_{ph}^{\mathbf{q}\alpha}(\mathbf{r}, t) \propto \exp(i\mathbf{q} \cdot \mathbf{r} - i\omega_{\mathbf{q}\alpha}t) A_{\mathbf{q}\alpha} b_{\mathbf{q}\alpha}^\dagger + h.c., \quad (86)$$

where $\mathbf{q}\alpha$ are the wavelength and the branch of the phononic modes, $A_{\mathbf{q}\alpha}$ is effective anisotropic piezo-electric modulus of wave $\mathbf{q}\alpha$. The matrix elements of the phonon Hamiltonian between the Zeeman split sublevels of orbital level n , that describe the spin-flip process with emission of phonon $\mathbf{q}\alpha$, are given at first order in the spin-orbit interaction by

$$\langle \Psi_n^\uparrow | U_{ph}^{\mathbf{q}\alpha} | \Psi_n^\downarrow \rangle = \sum_{k \neq n} \left[\frac{(U_{ph}^{\mathbf{q}\alpha})_{nk} (\mathcal{H}_{SO})_{kn}^{\uparrow\downarrow}}{E_n - E_k - g\mu_B B} + \frac{(U_{ph}^{\mathbf{q}\alpha})_{nk} (\mathcal{H}_{SO})_{kn}^{\downarrow\uparrow}}{E_n - E_k + g\mu_B B} \right]. \quad (87)$$

As a consequence of Kramer's theorem, in case of no external magnetic field, Eq. (87) is zero. Considering only Dresselhaus spin-orbit interaction, for small Zeeman splitting, $g\mu_B B \ll \sqrt{ms^2\hbar\omega_0}$, it is possible to obtain an effective spin-flip Hamiltonian which acts on the subspace of Zeeman sublevels of orbital level n , [19], where a phonon induced electric field arise as a gradient of U_{ph} . For a parabolic dot confinement potential, and for the particular case of circular dot with level spacing ω_0 , the spin-flip rate for the transition between the Zeeman sublevels of the dot ground state, associated with the emission of a piezo-phonon as depicted in Fig. 6, is [19]

$$\Gamma_1 = \frac{(g\mu_B B)^5}{\hbar(\hbar\omega_0)^4} \Lambda_p (1 + \cos^2(\vartheta)), \quad \Lambda_p \equiv \frac{2}{35\pi} \frac{(eh_{14})^2 \beta^2}{\rho \hbar} \left(\frac{1}{s_l^5} + \frac{4}{3s_t^5} \right), \quad (88)$$

where β is the strength of the Dresselhaus spin-orbit interaction, ϑ is the angle between the direction of confinement in the quantum dot z , and the direction of the applied magnetic field z' , and Λ_p is the strength of the effective spin-piezo-phonon coupling. For given longitudinal and transverse sound speed s_l and s_t , crystal mass density ρ , and modulus of the piezo-tensor eh_{14} ($eh_{14} = 1.3 \times 10^7$ eV/cm for GaAs), it ranges from $\approx 7 \times 10^{-3}$ to $\approx 6 \times 10^{-2}$, depending on β . Eq. (88) shows a strong dependence on the magnetic field and the lateral dot confinement energy ω_0 . For $\hbar\omega_0 = 10$ K and magnetic field $B = 1$ T, $\Gamma_1 \approx 1.5 \times 10^3 \text{s}^{-1}$. These theoretical expectations, in particular the B -dependence, have been confirmed in experiments [49–51], and long spin relaxation time, up to 1s, have been measured [21].

The effect of the Rashba spin-orbit interaction has so far not been taken into account. As the Dresselhaus term, it contributes to the admixing of spin and orbital states, and therefore to relaxation due to phonon scattering. The effect of the interplay of these two terms can show up in a strong difference in the their associated relaxation rates [21, 52–54]. For a quantum dot in external magnetic field, the first and second lowest levels show a crossing behavior as a function of the applied magnetic field, the ground state being not affected. In a perturbative treatment of the spin-orbit interaction [52], Dresselhaus and

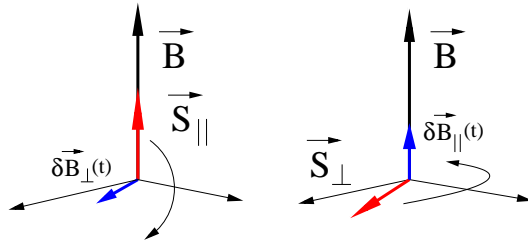


Figure 7. Schematic representation of the relaxation process (left side), due to magnetic field fluctuations $\delta B_{\perp}(t)$ orthogonal to the applied B field, and of the dephasing process (right side), due to magnetic field fluctuations $\delta B_{\parallel}(t)$ parallel to the applied B field.

Rashba terms show a qualitative difference, in which the latter couples the crossing levels, giving rise to an anticrossing of the levels at the point of accidental degeneracy. For magnetic fields much smaller than the crossing level value, the these two levels have a well defined spin orientation, i.e. low degree of admixture. In the region of anticrossing the admixture leads to complete superposition of the *up* and *down* states, and eventually to a reversed situation in the limit of magnetic field much larger than the crossing value, in which the two levels have again well defined spin, but reversed. Therefore, sweeping the magnetic field over the crossing region leads to spin-flip. In particular at the avoided crossing point, the strong admixture between spin states lead to a cusp-like behavior of the relaxation rate as a function of the magnetic field, at the anticrossing point.

1.15.2 Phonon-induced electron spin decoherence. In a Markovian dynamics the decoherence time T_2 is limited by both spin-flip and dephasing processes, though its upper bound is $T_2 \leq 2T_1$. A systematic analysis of phonon-induced spin decay is carried out in [55]. Also there both the Rashba and Dresselhaus spin-orbit interactions are treated perturbatively. The deformation potential phonons are also considered. For a spin-orbit length $\lambda_{SO} = \hbar/m^*\beta$ much larger than the electron orbit size λ , the contribution to the spin-phonon coupling in the Hamiltonian linear in $\lambda/\lambda_{SO} \propto \alpha, \beta$ is due only to a finite Zeeman splitting. For B field in the range $m^*\beta^2 \ll g\mu_B B \ll \hbar\omega_0$, the effective Hamiltonian is

$$\mathcal{H}_{\text{eff}} = \frac{1}{2}g\mu_B[\mathbf{B} + \delta\mathbf{B}(t)] \cdot \boldsymbol{\sigma}, \quad \delta\mathbf{B}(t) = 2\mathbf{B} \times \boldsymbol{\Omega}(t), \quad (89)$$

where $\boldsymbol{\Omega}(t) = \langle \psi | [(\hat{L}_d^{-1}\boldsymbol{\xi}), U_{\text{ph}}(t)] | \psi \rangle$, $|\psi\rangle$ is the electron orbital wave function, \hat{L}_d is the dot Liouvillian, $\hat{L}_d A = [\mathcal{H}_d, A]$. The vector $\boldsymbol{\xi}$ lies in the 2D dot plane and depends on α , β , and m^* . The most important consequence of Eq. (89) is

that within first order in the spin-orbit coupling parameter there can only be transverse fluctuations of the effective field.

In case of many uncorrelated scattering events, the expectation values $\langle \mathbf{S} \rangle$ of the spin obeys the Bloch equation [6]

$$\langle \dot{\mathbf{S}} \rangle = \boldsymbol{\omega} \times \langle \mathbf{S} \rangle - \Gamma \langle \mathbf{S} \rangle + \boldsymbol{\Upsilon}, \quad (90)$$

where $\boldsymbol{\omega} = \omega \mathbf{B}/B$, $\omega = g\mu_B B/\hbar$. In the Born-Markov approximation, for a generic $\delta \mathbf{B}$ such that $\langle \delta \mathbf{B} \rangle = 0$, the tensor Γ can be expressed in terms of the spectral function

$$J_{ij}(\omega) = \frac{g^2 \mu_B^2}{2\hbar^2} \int_0^\infty dt \langle \delta B_i(0) \delta B_j(t) \rangle e^{-i\omega t}, \quad (91)$$

and it is diagonal in a frame (X, Y, Z) , with Z oriented along \mathbf{B} . The symmetric part of Γ is responsible for the decay of the spin components, and it can be expressed just as function of $J_{ij}^\pm(\omega) = \text{Re}[J_{ij}(\omega) \pm J_{ij}(-\omega)]$. Γ can be split in two contributions, $\Gamma = \Gamma^r + \Gamma^d$, where Γ^r contains the spectral function $J_{ij}(\omega)$ at the Zeeman frequency ω , and describes spin decay due to emission or absorption of a phonon, whereas Γ^d is due to elastic scattering of spin. The relaxation time T_1 is completely determined by Γ^r , while the decoherence time T_2 is affected by both Γ^r and Γ^d , the latter describing pure dephasing. In the general case, solution of Eq. (90) yields

$$\frac{1}{T_1} := \Gamma_{ZZ} = \Gamma_{ZZ}^r, \quad \frac{1}{T_2} := \frac{1}{2}(\Gamma_{XX} + \Gamma_{YY}). \quad (92)$$

In many cases the contribution of Γ^r to spin decoherence is negligible, the decoherence rate being determined entirely by Γ^d . However, it turns out that, at first order perturbation theory in the spin-orbit interaction, no dephasing takes place [55]. Due to the transverse nature of the fluctuations in the magnetic field in the effective Hamiltonian, the tensor Γ^d is identically zero, $\Gamma^d = 0$ (Fig. 7 illustrates an intuitive picture of the effect of the longitudinal and the transverse fluctuations). As a result

$$\frac{1}{T_1} = \frac{2}{T_2} = J_{XX}^+(\omega) + J_{YY}^+(\omega). \quad (93)$$

Contributions to the decoherence time T_2 due to pure dephasing arise when two-phonon processes are taken into account in the next order in the electron-phonon interaction [56]. Therefore, if only spin-orbit decay mechanisms are taken into account, the decoherence time T_2 for the decay of the transverse

component of an electron spin in GaAs quantum dots is $T_2 = 2T_1$.

1.16 Spin-orbit interaction for heavy holes

The electron spin in GaAs quantum dots has shown to have a long relaxation time, due to inefficient phonon-induced relaxation mechanisms. On the other hand, the decoherence time is mainly dominated by hyperfine induced decay, due to the fact that the decay of the longitudinal electron spin component can be strongly suppressed by the application of an external magnetic field. In order to circumvent this problem, the use of hole spins as carriers has been recently proposed. The valence band in III-V semiconductors has a p symmetry, for which the electron has zero probability to be found on the position of the nucleus. According to Eq. (51), it follows that the hyperfine interaction between holes and nuclei is strongly suppressed with respect to that of nuclei and conduction band electrons. However, the hole spin relaxation time turns out to be much smaller than that of the electrons by several order of magnitude. The reason for this is due to the fact that, beside the spin-orbit coupling due to bulk inversion asymmetry and the structural inversion asymmetry, there is a strong spin-orbit coupling between the heavy-holes (HH) and the light-holes (LH) sub-bands [57]. Investigations of hole spin relaxation in quantum dots, exclusively due to spin-orbit coupling of LH and HH sub-bands, give estimates for the relaxation time much shorter than the case for electron spin [58, 59].

In Ref. [64], HH spin relaxation is analyzed in presence of Rashba and Dresselhaus spin-orbit coupling, as well as spin-orbit between HH and LH. From the two-band Kane model, the Hamiltonian for the valence band of III-V semiconductors is given by

$$\mathcal{H}_{\text{bulk}} = \mathcal{H}_{\text{LK}} + \eta \mathbf{J} \cdot \boldsymbol{\Omega} + \mathcal{H}_Z, \quad (94)$$

where \mathcal{H}_{LK} is the Luttinger-Kohn Hamiltonian [60], $\eta \propto (E_g + \Delta_{\text{so}})/\Delta_{\text{so}}$, Δ_{so} is the split-off gap energy, and E_g is the band gap energy. $\mathbf{J} = (J_x, J_y, J_z)$ are the 4×4 matrices corresponding to spin 3/2, $\Omega_z = P_z(P_x^2 - P_y^2)$, and Ω_x, Ω_y are obtained by cyclic permutations. The last term in Eq. (94) $\mathcal{H}_Z = -2\kappa\mu_B \mathbf{B} \cdot \mathbf{J} - 2q\mu_B \mathbf{B} \cdot \mathcal{J}$ is the Zeeman term for the valence band [61], with κ and q Luttinger parameters [61], and $\mathcal{J} = (J_x^3, J_y^3, J_z^3)$.

In case of structure inversion asymmetry along the growth direction, due to an asymmetric confinement, there is an additional contribution to the spin-orbit interaction, the Bychkov-Rashba term. For the two-band Kane model it is given by [62, 63] $\alpha_R(\mathbf{P} \times \mathbf{E}) \cdot \mathbf{J}$, where \mathbf{E} is the effective electric field along the growth direction, and α_R is the Bychkov-Rashba spin-orbit coupling constant. We consider a two-dimensional system grown along the [001]-direction. Be-

cause of confinement, the valence band splits into a heavy-hole subband, with $J_z = \pm 3/2$, and a light-hole subband, with $J_z = \pm 1/2$ [57,64], where z is the growth direction. In case of large splitting Δ between HH and LH, the properties of the two subbands can be described separately, the $J_z = \pm 3/2$ subspace for HHs and the $J_z = \pm 1/2$ subspace for LHs, using only the 2×2 submatrices. The HHs submatrices have the properties $\tilde{J}_x = \tilde{J}_y = 0$, and $\tilde{J}_z = \frac{3}{2}\sigma_z$ [65]. For low temperatures only the HH subband is significantly occupied. Considering only HHs, starting from the bulk Hamiltonian Eq. (94) with the addition of the Bychkov-Rashba term, at the lowest order in perturbation theory [66], it is possible to derive an effective Hamiltonian for a quantum dot with lateral confinement potential $U(x, y)$

$$\mathcal{H} = \frac{1}{2}(P_x^2 + P_y^2) + U(x, y) + \mathcal{H}_{\text{SO}}^{\text{HH}} - \frac{1}{2}g_{zz}\mu_B B_z \sigma_z, \quad (95)$$

where m is the effective HH mass, g_{zz} is the component of the g factor tensor along the growth direction, and the effect of an in-plane component of the magnetic field can be neglected due to strong anisotropy in the HH g factor, $g_{\parallel} \ll g_{zz}$ [65], as well as the orbital effect of the in-plane magnetic field, as long as $B_{\parallel} \ll c\hbar/eh^2$, h being the height of the quantum dot. $\mathbf{P} = \mathbf{p} + (|e|/c)\mathbf{A}(\mathbf{r})$, with $\mathbf{A}(\mathbf{r}) = (-yB_z/2, xB_z/2, yB_x - xB_y)$, and

$$\mathcal{H}_{\text{SO}}^{\text{HH}} = i\alpha\sigma_+P_-^3 + \beta P_-P_+P_- \sigma_+ + \gamma B_-P_-^2\sigma_+ + \text{h.c.} \quad (96)$$

The first two terms in the spin-orbit interaction for heavy holes consist in the Rashba and Dresselhaus contribution, respectively, while the last term (γ) describes the combination of two effects: the orbital coupling via non-diagonal elements in the Luttinger-Kohn Hamiltonian ($\propto P_{\pm}^2$), taken into account perturbatively, and magnetic coupling via non-diagonal elements in the Zeeman term, ($\propto B_{\pm}$) [61]. This new spin-orbit term is unique for heavy holes [67]. In Eq. (96) $\alpha = 3\gamma_0\alpha_R\langle E_z \rangle/2m_0\Delta$, $\beta = -3\gamma_0\eta\langle P_z^2 \rangle/2m_0\Delta$, $\gamma = 3\gamma_0\kappa\mu_B/m_0\Delta$, $\sigma_{\pm} = (\sigma_x \pm \sigma_y)/2$, $P_{\pm} = P_x \pm P_y$, and $B_{\pm} = B_x \pm B_y$, m_0 is the free electron mass, γ_0 is the Luttinger parameter [61], $\langle E_z \rangle$ is the average electric field, and Δ is the splitting between heavy and light hole subbands, $\Delta \propto h^{-2}$, where h is the quantum-dot height. For a quantum dot with characteristic lateral size l , the ratio $\langle \mathcal{H}_{\text{SO}}^{\text{el}} \rangle / \langle \mathcal{H}_{\text{SO}}^{\text{HH}} \rangle \propto (l/h)^2$. Therefore for flat quantum dots, $l/h \gg 1$, the spin-orbit coupling for heavy holes can be weaker than that for conduction electrons [52,55]. This observation has also been confirmed experimentally [68], where the spin relaxation rate for heavy holes has shown to be comparable to that of electrons.

For vanishing spin-orbit interaction, the spectrum of the Hamiltonian Eq. (95) for a parabolic lateral confinement can be found through a canonical

transformation [69], and it is the Fock-Darwin spectrum split by the Zeeman term [70, 71]. In the framework of perturbation theory [52], it can be seen that the corrections to the spectrum due to $\mathcal{H}_{\text{SO}}^{\text{HH}}$ arise only at second order, and the spin-orbit interaction influences the wave functions more strongly than the energy levels. $\mathcal{H}_{\text{SO}}^{\text{HH}}$ couples the two lowest states $|0, \pm 3/2\rangle$ to the states with opposite spin orientations and different orbital momenta $|l, \mp 3/2\rangle$. The different spin-orbit interactions appearing in Eq. (96) differ by symmetry in the momentum space [52, 72], and thus produce a mixing of spin-up and spin-down states, with resulting avoided crossings between energy levels. We mention here that the levels cross only if $g_{zz} > 0$, therefore in case of GaAs ($g_{zz} > 0$) quantum dots an anticrossing appears, with consequent peak of the relaxation rate as a function of the magnetic field, at the point where the crossing takes place, while for InAs ($g_{zz} < 0$) quantum dot no crossing and no cuspic-like behavior of the relaxation rate appear. The spin-orbit mixing of the heavy-hole states provides a mechanism of transitions between the states $|0, \pm 3/2\rangle$ through emission or absorption of an acoustic phonon, that ultimately represents the main source of relaxation and decoherence for heavy-holes [64].

Taking into account piezoelectric and deformation potential phonons, the potential of a phonon with mode $\mathbf{q}\alpha$ is given by [19, 66]

$$U_{\mathbf{q}\alpha}^{\text{ph}} = \sqrt{\frac{\hbar}{2\rho s_{\alpha} q V}} F(q_z) e^{i\mathbf{q}_{\parallel} \cdot \mathbf{r}} \times \left\{ w A_{\mathbf{q}\alpha} + i \left[\left(a + \frac{b}{2} \right) \mathbf{q} \cdot \mathbf{d}^{\mathbf{q}\alpha} - \frac{3}{2} b q_z d_z^{\mathbf{q}\alpha} \right] \right\}, \quad (97)$$

where $\mathbf{q}_{\parallel} = (q_x, q_y)$, a and b are constants of the deformation potential, V the quantum dot volume, s_{α} the sound velocity, ρ the crystal mass, $A_{\mathbf{q}\alpha}$ the effective piezoelectric modulus, $\mathbf{d}_{\mathbf{q}\alpha}$ the phonon polarization vector, $F(q_z)$ the form factor, which is determined by the spread of the electron wave function in the z direction.

1.16.1 Spin decoherence and relaxation for heavy holes. For a single-particle quantum dot, in which an heavy hole can occupy one of the low-lying levels, some energy levels with same spin orientation cross, with increasing B , the upper Zeeman-split ground state level. Therefore we consider an n -level system, in which the first $n - 1$ levels have same spin orientation, while the n -level has opposite spin. In the context of Bloch-Redfield theory, the Bloch equations for the spin motion of a heavy hole in such a system are given, in the interaction picture, by

$$\langle \dot{S}_z \rangle = (S_T - \langle S_z \rangle) / T_1 - R(t), \quad (98)$$

$$\langle \dot{S}_x \rangle = -\langle S_x \rangle / T_2, \quad \langle \dot{S}_y \rangle = -\langle S_y \rangle / T_2, \quad (99)$$

where $R(t) = W_{n1}\rho_{nn}(t) + \sum_{i=1}^{n-1} W_{ni}\rho_{ii}(t)$, $\rho(t)$ is the density matrix, W_{ij} is the transition rate from state j to state i , S_T is a constant that takes the value $\langle S_z \rangle$ in the thermodynamic equilibrium $R(t) = 0$, and

$$\frac{1}{T_1} = W_{n1} + \sum_{i=1}^{n-1} W_{in}, \quad \frac{1}{T_2} = \frac{1}{2T_1} + \frac{1}{2} \sum_{i=1}^{n-1} W_{i1}, \quad (100)$$

where the pure dephasing term, which is due to fluctuations along the longitudinal z direction, is absent in the decoherence time T_2 , because the spectral function is superohmic. The spin motion involves $n - 1$ states and therefore there are $n - 1$ transition rates. It can be shown, by solving the master equation, that for low temperature $\hbar q_\alpha \gg k_B T$, $R(t) \approx 0$ and phonon absorption is strongly suppressed. In this case only one relaxation rate contributes to relaxation time T_1 . In this limit the last sum in the expression for the decoherence rate can be neglected, and the decoherence time T_2 saturates, $T_2 = 2T_1$. The relaxation rates for the different spin-orbit interactions are [64]

$$\frac{1}{T_1^{\text{BR}}} \propto \alpha^2 \omega_z^7 \left(\frac{\omega_+^3}{3\omega_+ + \omega_Z} - \frac{\omega_-^3}{3\omega_- - \omega_Z} \right)^2, \quad (101)$$

$$\frac{1}{T_1^{\text{D}}} \propto \beta^2 \omega_z^3 \left(\frac{\omega_+}{\omega_+ + \omega_Z} - \frac{\omega_-}{\omega_- - \omega_Z} \right)^2, \quad (102)$$

$$\frac{1}{T_1^{\parallel}} \propto \gamma^2 B_{\parallel}^2 \omega_z^5 \left(\frac{\omega_+^2}{2\omega_+ + \omega_Z} + \frac{\omega_-^2}{2\omega_- - \omega_Z} \right)^2, \quad (103)$$

where $\omega_{\pm} = \Omega \pm \omega_c/2$, $\Omega = \sqrt{\omega_0^2 + \omega_c^2/4}$, $\omega_c = |e|B/mc$ is the cyclotron frequency, $\omega_Z = g_{zz}\mu_B B_z$, and $B_{\parallel} = \sqrt{B_x^2 + B_y^2}$. In contrast to the case of conduction electrons [55], no interference takes place for heavy holes, and the rates originating from different spin-orbit terms sum up, giving the total spin relaxation rate $1/T_1 = 1/T_1^{\text{BR}} + 1/T_1^{\text{D}} + 1/T_1^{\parallel}$. For the case of GaAs quantum dots the crossing between levels takes place at $\omega_Z = \omega_-$, $2\omega_-$, and $3\omega_-$, and the strong spin mixing arising causes cuspic-like peaks in the relaxation rate as a function of the external field B .

1.16.2 Electric dipole spin resonance for heavy holes. The possibility of coherent manipulating the spins is of great importance for spintronics and quantum computation. In case of conduction electron spin-based electronics, such control is obtained by the electron spin resonance (ESR). Through the

application of short resonant microwave pulses, arbitrary superpositions of spin-up and spin-down states can be created. Therefore ESR provides a necessary tool for single-qubit operations, an essential requirement for quantum computation. In Rabi oscillations and spin echo experiments [73], that are based on this technique, the ESR signal can be detected by measuring the absorption of radio-frequency (rf) power [74]. ESR methods involve magnetic-dipole transitions induced by oscillating magnetic fields. Besides, an alternative is provided by alternating electric fields, that give rise to electric-dipole spin resonance (EDSR).

Considering the spin-orbit coupling as a perturbation, at first order the two states corresponding to the Zeeman-split ground state $|\pm\rangle$ are given as a superposition of few unperturbed Fock-Darwin states and spin states, $|n, \ell\rangle|s\rangle$, with $n \in \mathbb{N}$ the principal quantum number, $|\ell| \leq n$ the azimuthal quantum number, and $s = \pm 3/2$, for a detailed see Ref. [67]. In the case of heavy holes it can be shown [67] that magnetic-dipole transition ($\Delta n = 0$, $\Delta \ell = 0$, and $\Delta s = \pm 1$) are forbidden, while, because of spin-orbit coupling between states with different orbital momenta and opposite spin orientations, $|0, 0, \pm 3/2\rangle$ and $|1, \pm 1, \mp 3/2\rangle$, electric-dipole transitions ($\Delta n = \pm 1$, $\Delta \ell = \pm 1$, and $\Delta s = 0$) are most likely to occur. Heavy holes are thus affected by the oscillating electric field component, but not by the magnetic one. EDSR for heavy hole appears to be an essential tool for the control of spin dynamics and for the determination of important parameters, as the effective g factor, effective mass m , spin-orbit coupling constants, and spin relaxation and decoherence time.

The Hamiltonian for the interaction of HHs with a circularly polarized electric field, that rotates with frequency ω in the XY -plane, $\mathbf{E}(t) = E(\sin \omega t, -\cos \omega t, 0)$, is given by $\mathcal{H}^E = (|e|E/m\omega)(P_x \cos \omega t + P_y \sin \omega t)$. The coupling between the states $|\pm\rangle$ is given by $\langle +|\mathcal{H}^E|-\rangle = d_{\text{SO}} E e^{-i\omega t}$, where

$$d_{\text{SO}} = (|e|l/2\omega)(\beta_1^+ \omega_+ + \beta_1^- \omega_-), \quad (104)$$

is an effective dipole moment of a heavy hole and it depends on Dresselhaus spin-orbit coupling constant, perpendicular magnetic field B_\perp , lateral quantum dot size, and frequency ω of the rf electric field. For details on β_1^\pm and l see Ref. [67].

The effective master equation for the density matrix ρ_{nm} , in the context of Bloch-Redfield theory, takes the form of Bloch equations, with a rf field detuned from ω_Z , $\delta_{\text{rf}} = \omega_Z - \omega$, Larmor frequency $2d_{\text{SO}}E/\hbar$, spin relaxation time $T_1 = 1/(W_{+-} + W_{-+})$, W_{nm} being the transition rate from state m to state n , decoherence time $T_2 = 2T_1$, and equilibrium value of ρ_z without rf field given by $\rho_z^T = (W_{+-} - W_{-+}T_1)$.

The coupling energy between a heavy hole and an oscillating field is given

by

$$\langle \mathcal{H}^E(t) \rangle = -\mathbf{d}_{\text{SO}} \cdot \mathbf{E}(t), \quad (105)$$

where $\mathbf{d}_{\text{SO}} = d_{\text{SO}}(i\rho_{-+} - i\rho_{+-} + \rho_{-+}, 0)$ is the dipole moment of a heavy hole. The rf power $P = -d\langle \mathcal{H}^E(t) \rangle / dt = -\omega d_{\text{SO}} E \rho_-$ absorbed by a heavy hole spin system in a stationary state is given by [75]

$$P = \frac{2\omega(d_{\text{SO}}E)^2 T_2 \rho_z^T / \hbar}{1 + \delta_{\text{H}}^2 T_2^2 + (2d_{\text{SO}}E/\hbar)^2 T_1 T_2}. \quad (106)$$

The dependence of P on perpendicular magnetic field B_{\perp} and frequency of the oscillating field ω shows three resonances and one resonant dip. The first resonance corresponds to the Zeeman energy of the heavy hole $B_{\perp} = \hbar\omega/g_{\perp\mu_B}$, the second to the first anticrossing between the unperturbed $E_{0,-3/2}$ and $E_{1,3/2}$ energy levels, $\omega_Z - \omega_-$, the third resonance reflects the peak in the decoherence rate T_2^{-1} due to an applied in-plane magnetic field at the second anticrossing $\omega_Z = 2\omega_-$. The resonant dip takes place at zero dipole moment.

The study of the position of these resonance allows to determine g_{\perp} , m , and ω_0 , while the shape and height provide information about the spin-orbit interaction constants α , β , and spin-orbit interaction strength due to in-plane magnetic field. Besides, it is possible to extract informations about the dependence of spin relaxation and decoherence times on B_{\perp} .

1.17 Superconducting qubits

Besides spin qubits in semiconductor quantum dots, superconducting qubits represent a category of promising candidates for the implementation of artificial two-level systems as qubits. The key ingredient in building superconducting qubits is the strong nonlinearity of the current-voltage relation of a Josephson junction. The ability to isolate few charge states on a superconducting island, together with the possibility to let them interact through the coherent tunneling of Cooper pairs through the junction, represent a promising way to control a operate a purely quantum system (charge qubits). The flux quantization together with the strong nonlinear potential, arising from the current-voltage relation, provide a way to isolate few current states and coherently superimpose them (flux qubit).

Superconducting qubits can be included in a more general framework of quantum circuits, that are electrical circuits showing, in the low temperature regime, quantum behavior, including quantum fluctuations [76]. In this context, as LC -circuits provide electrical realizations of quantum harmonic oscillators, showing a linear current-voltage relation, Josephson junctions provide

a full anharmonic counterpart, showing a more rich spectrum, with groups of few energy levels well separated from higher bands of the spectrum.

Several types of superconducting qubits based on Josephson junctions have been so far theoretically proposed and experimentally realized (for comprehensive reviews see [77, 78]). Apart from the particular design of each device, superconducting qubits can be classified according of the working regime of the Josephson elements that constitutes the circuit. Every Josephson junction is characterized by two features: i) a critical current I_c , that is the maximal supercurrent that can flow through the junction; and ii) an effective capacitance that the two superconducting faces have to accumulate charge. Together the energy associated with the critical current $E_J = I_c \Phi_0 / 2\pi$ and the charging energy of the associated capacitance $E_C = e^2 / 2C$ are the two most important parameters that determine the qubit working regime. For $E_C \gg E_J$ the charge degrees of freedom are well defined and the number of Cooper pairs in a superconducting island is a well defined quantum number. Qubits that work in this regime are called charge qubits [79–88]. To the contrary, for $E_C \ll E_J$ flux degrees of freedom have well defined values, and current states are well defined. Qubits that operate in this regime are called flux qubits [89–92]. Other realizations of superconducting qubits, for different values of the ratio E_J / E_C , and many kind of possible accessible parameter regimes have been explored. The so called phase qubit [93, 94] operates in the flux regime, but is completely represented by the superconducting phase, and it has no magnetic flux or circulating current associated. The quantronium [95], consisting of a split Cooper pair box arranged in a loop containing an extra large junction for the read-out.

Experimental observation of Rabi oscillations in driven quantum circuits have shown several periods of coherent oscillations, confirming, to some extent, the validity of the two-level approximation and possibility of coherently superimpose the computational two states of the system. Nevertheless, the unavoidable coupling to a dissipative environment surrounding the circuit represents a source of relaxation and decoherence that limit the performances of the qubit for quantum computation tasks. Therefore, for the implementation of superconducting circuits as quantum bits, it is necessary to understand the way the system interacts with the environmental degrees of freedom, and to reduce their effect, if possible.

1.18 *Circuit theory and system Hamiltonian*

A systematic approach to obtain the Lagrangian of a generic circuit containing many different lumped elements, as well as Josephson junctions, has been proposed in [96, 97]. In this way, it is possible to construct the full classical Hamiltonian of the system, quantize it and study its quantized spectrum, in

the two-level approximation.

1.18.1 Network graph theory and the equations of motion. By means of classical network theory, an electric circuit is represented by an oriented graph, consisting of nodes and branches. Each branch correspond to a single two-terminal element, such as resistor, capacitor, inductor, current source, voltage source, etc.. The branches are then divided into two groups, the tree, representing a set of branches of the graph connecting all nodes without containing any loop, and the chords, represented by all the rest of branches. This way every time a chord branch is added to the tree a loop is obtained. The grouping in chords and tree depends on the formalism adopted, that in turn is functional to the kind of circuit described, either a flux qubit or a charge qubit. All the the topological information of the circuit is contained in the fundamental loop matrix \mathbf{F} , that connects tree branches and loops (i.e. chords), such that the matrix elements F_{XY} can be 1, -1, 0, depending whether the tree branch X and the chord branch Y have the same orientation, different orientation in the loop, or do not belong to the same loop.

The equations of motion are represented by Kirchhoff's laws, and can be at once written as

$$\mathbf{F}\mathbf{I}_{\text{ch}} = -\mathbf{I}_{\text{tr}}, \quad \mathbf{F}^T\mathbf{V}_{\text{tr}} = \mathbf{V}_{\text{ch}} - \dot{\Phi}_{\text{ext}}. \quad (107)$$

Here $\dot{\Phi}_{\text{ext}}$ takes into account the possibility of having time dependent applied external fluxes. The fluxes and charges of the circuit represent the canonical variables of system, and they can be formally defined for the generic element X as

$$\mathbf{I}_X(t) = \dot{\mathbf{Q}}_X(t), \quad \mathbf{V}_X(t) = \dot{\Phi}_X(t). \quad (108)$$

From the last equation and from the second Josephson relation, it is possible to identify the formal flux associated to the Josephson junction as the superconducting phase difference φ across the junction,

$$\frac{\Phi_J}{\Phi_0} = \frac{\varphi}{2\pi}, \quad \mathbf{I}_J = \mathbf{I}_c \sin\varphi, \quad (109)$$

where the second formula represents the first Josephson relation. With current-voltage relations for the various types of other branches, it is possible to obtain the classical equations of motion for the superconducting phases

$$\mathbf{C}\ddot{\varphi} = -\mathbf{L}_J^{-1}\sin\varphi - \mathbf{M}_0\varphi - \mathbf{M}_d * \varphi - \frac{2\pi}{\Phi_0}(\mathbf{N}\Phi_{\text{ext}} + \mathbf{S}\mathbf{I}_B), \quad (110)$$

where $\mathbf{L}_J^{-1} = 2\pi\mathbf{I}_c/\Phi_0$ is a diagonal matrix for the Josephson inductances of the junctions, \mathbf{M}_0 is the matrix of linear inductance, describing their energy and mutual interaction, \mathbf{N} and \mathbf{S} describing the inductive coupling of the phases φ with external fluxes and currents, respectively. $\mathbf{M}_d(t)$ is a symmetric matrix containing all the dissipative dynamics of φ , [96].

1.18.2 Two-level approximation. Dissipative elements present in the circuit are incompatible with a Hamiltonian description of the system, therefore for the moment we omit them. In order to derive the Lagrangian for the electric circuit, a complete set of unconstrained flux and charge degrees of freedom has to be isolated, such that every assignment of values to those charges and fluxes represents a possible dynamical state of the system. The Hamiltonian of the circuit follows straightforwardly from the Lagrangian by means of a Legendre transformation, and can be formally written as

$$\mathcal{H} = \frac{1}{2}(\mathbf{Q} - C_{\mathbf{V}}\mathbf{V})^T \mathbf{C}^{-1}(\mathbf{Q} - C_{\mathbf{V}}\mathbf{V}) + \left(\frac{\Phi_0}{2\pi}\right)^2 U(\varphi), \quad (111)$$

$$U(\varphi) = -\sum_i \frac{2\pi I_{c;i}}{\Phi_0} \cos \varphi_i + \frac{1}{2}\varphi^T \mathbf{M}_0 \varphi + \frac{2\pi}{\Phi_0} \varphi^T (\mathbf{N}\Phi_{\text{ext}} + \mathbf{S}\mathbf{I}_B), \quad (112)$$

where \mathcal{C} is the capacitance matrix, collecting all the capacitive elements of the circuit, and describing the effective charge energy of the system, $C_{\mathbf{V}}$ describes the coupling of the charges \mathbf{Q} to externally applied voltages \mathbf{V} , The number of Cooper pair, that accumulates on a junction capacitance, and the phase of the superconducting order parameter through the junction, for sufficiently low temperatures, become quantized and satisfy canonical commutation rules,

$$\left[\hat{\Phi}_i, \hat{Q}_j \right] = \left[\frac{\Phi_0}{2\pi} \hat{\varphi}_i, 2e\hat{N}_j \right] = i\hbar\delta_{ij}, \quad (113)$$

where $2e$ is the charge of a Cooper pair, and $\Phi_0/2\pi$ is flux quantum. Therefore, once a Hamiltonian is obtained from circuit theory, its quantization follows straightforwardly. The energy of an isolated system is a conserved quantity, therefore strictly speaking the Hamiltonian should be time independent. However time-dependent circuit elements, such as alternating currents and voltages, can be included in the Hamiltonian description as time-dependent parameters.

Care should be taken when dissipative elements such as resistors are present in the circuit. In this case a more general approach must be adopted, in which the system considered is coupled to an environmental bath, and the dynamics of

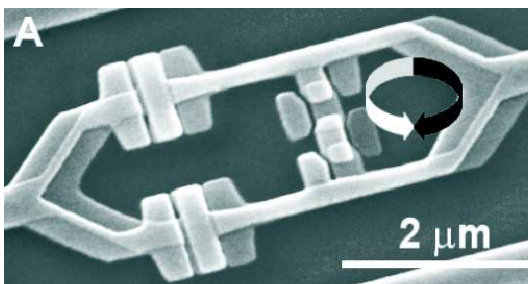


Figure 8. Scanning electron micrograph of the Delft flux qubit (small loop with three Josephson junctions) and attached SQUID (large loop) [92] (With permission from the Authors).

the circuit under analysis is obtain as the dynamics of part of a larger isolated system, as discussed in section 1.5.

Once the Hamiltonian has been obtained and quantized it is possible to study the temperature regime, in which few low energy states are taken into consideration. A two-level approximation can be carried out by considering only the ground state and first excited state, and neglecting higher levels of the spectrum. The goodness of the two-level approximation is controlled by the ratio of the temperature and the energy gap between the first and second excited state, $k_B T / \Delta_{12} \ll 1$. The Hamiltonian of the two-level system can be therefore expressed in the form of a pseudo-spin 1/2

$$\mathcal{H} = \frac{\Delta}{2} \sigma_x + \frac{\epsilon}{2} \sigma_z, \quad (114)$$

where Δ denotes the tunnel coupling between the two qubit states $|0\rangle$ and $|1\rangle$, eigenstates of σ_z , and ϵ the bias, due to asymmetry.

1.19 Decoherence in superconducting qubits

In this section we choose to describe decoherence effects in only two realizations of superconducting qubits, namely the phase qubit [93, 94] and the flux qubit [89, 96, 98]. An extensive treatment of decoherence in the quantronium circuit is carried out in [99].

1.20 The superconducting persistent current qubit: Delft qubit

In the working regime $E_J \gg E_C$, three types of circuit designs have been proposed, the Delft flux qubit [89, 92], the IBM flux qubit [96], and its gradiometer variety [98]. The phase qubit operates in the same regime, see Sec. 1.21

The flux qubit realized at Delft [92] consists of a superconducting loop in-

errupted by three Josephson junctions (see Fig. 8). The strong flux regime $E_J \gg E_C$ allows flux quantization of the flux through the loop, $\varphi_1 + \varphi_2 + \varphi_3 = 2\pi n$. Therefore, only two of the three phases of the junctions play the role of dynamical variables. For sufficiently low temperatures, in the small loop inductance limit, the inductive degree of freedom associated with the loop is frozen, and the effective potential $U(\varphi)$ is periodic and shows a double well shape. The charging energy of the system here plays the role of the kinetic energy, and the Hamiltonian is written as

$$\mathcal{H} = -2e^2 \nabla_{\varphi}^T \mathcal{C}^{-1} \nabla_{\varphi} + \left(\frac{\Phi_0}{2\pi} \right)^2 U(\varphi). \quad (115)$$

The lowest energy states are two flux states localized in the two well minima φ_L and φ_R , and they correspond to clockwise and counter clockwise circulating currents in the loop, $|L\rangle$ and $|R\rangle$, encoding the logical $|0\rangle$ and $|1\rangle$ states of the qubit. Tunneling through the potential barrier between the wells lifts the degeneracy between the two current states, giving rise to a splitting $\Delta = \langle L | \mathcal{H} | R \rangle$ between the lowest states of the system, that become the symmetric and symmetric superpositions of the current states. An external bias flux can create asymmetry in the double well, $\epsilon = \langle L | \mathcal{H} | L \rangle - \langle R | \mathcal{H} | R \rangle$. The qubit Hamiltonian written in the $\{|L\rangle, |R\rangle\}$ basis takes the form

$$\mathcal{H} = \frac{\Delta}{2} \sigma_x + \frac{\epsilon}{2} \sigma_z. \quad (116)$$

1.20.1 Markovian dynamics due to dissipative circuitry. The regime of working of flux qubits, in which the charging energy is much smaller than the Josephson energy, $E_C \ll E_J$, makes the flux qubits substantially insensitive to background charge fluctuations. Still, however, other mechanisms can affect their phase coherence and in order to implement them as building blocks for quantum computation schemes, it is necessary to understand which sources of decoherence affect the short time dynamics of flux qubits and reduce as much as possible their effect.

Several sources of dissipation for flux qubits have been discussed throughout the literature [100], background charge fluctuations ($\tau_{\varphi} \approx 0.1\text{s}$), as well as quasiparticle tunneling in the superconductor with a non-vanishing subgap conductance ($\tau_{\varphi} \approx 1\text{ms}$). Nuclear spins in the substrate have also been considered as a possible source of dissipation. Static random magnetic field produced by the nuclear spins may induce shifts in qubit frequencies, but no dephasing is expected until a typical nuclear relaxation time, which can be very long, up to minutes, due to the slow dynamics of nuclear spins.

However, the most efficient source of dissipation for flux qubits is represented by fluctuations in the external circuit that produce fluctuating magnetic fluxes through the loop. The coupling of flux degrees of freedom of the qubit to the dissipative environmental elements is well described in the graph formalism described in [96]. In the Born-Markov approximation, it can be shown that the Redfield tensor, written in the eigenbasis $\{|n\rangle\}$ of \mathcal{H}_S , is entirely determined by

$$\text{Re}\Gamma_{lmnk}^{(+)} = (\mathbf{m} \cdot \boldsymbol{\varphi})_{lm} (\mathbf{m} \cdot \boldsymbol{\varphi})_{nk} J(|\omega_{nk}|) \frac{e^{-\beta\omega_{nk}/2}}{\sinh \beta|\omega_{nk}|/2}, \quad (117)$$

$$\text{Im}\Gamma_{lmnk}^{(+)} = -(\mathbf{m} \cdot \boldsymbol{\varphi})_{lm} (\mathbf{m} \cdot \boldsymbol{\varphi})_{nk} J(|\omega_{nk}|) \frac{2}{\pi} P \int_0^\infty d\omega \frac{J(\omega)}{\omega^2 - \omega_{nk}^2} \quad (118)$$

$$\times \left(\omega - \omega_{nk} \coth \frac{\beta\omega}{2} \right), \quad (119)$$

where $\beta = k_B T$ and the $\mathbf{m} \cdot \boldsymbol{\varphi}$ appears in the Hamiltonian for the system-bath coupling, \mathbf{m} being related to the topology of the dissipative circuitry.

In the two-level approximation, the rates for transitions from the two-level subspace to higher states can be neglected, and Eqs. (117) and (119) simplify and the dynamics of the 2×2 density matrix of the system can be cast in the form of Bloch equations for the dynamics of a pseudo spin 1/2. In this framework the relaxation matrix contains just two rates, T_1^{-1} and T_2^{-1} for the decay of the longitudinal and transverse pseudo spin component, respectively. The latter in turn is limited by relaxation time T_1 and pure dephasing time T_ϕ , $1/T_2 = 1/2T_1 + 1/T_\phi$, and the two rates are given by [96]

$$\frac{1}{T_1} = 4|\langle 0|\mathbf{m} \cdot \boldsymbol{\varphi}|1\rangle|^2 J(\omega_{01}) \coth \frac{\omega_{01}}{2k_B T}, \quad (120)$$

$$\frac{1}{T_\phi} = |\langle 0|\mathbf{m} \cdot \boldsymbol{\varphi}|0\rangle - \langle 1|\mathbf{m} \cdot \boldsymbol{\varphi}|1\rangle|^2 \left. \frac{J(\omega)}{\omega} \right|_{\omega \rightarrow 0} 2k_B T. \quad (121)$$

Typically, T_ϕ can be made to diverge for an appropriate choice of external fluxes such that $\langle 0|\mathbf{m} \cdot \boldsymbol{\varphi}|0\rangle = \langle 1|\mathbf{m} \cdot \boldsymbol{\varphi}|1\rangle$. However, this divergence is not expected to show up experimentally, since it will be cut off by other mechanisms.

The two lowest energy states, eigenstates of the Hamiltonian Eq. (116), are

given by

$$|0\rangle = \frac{1}{\sqrt{2}} \left(\sqrt{1 + \frac{\epsilon}{\omega_{01}}} |L\rangle + \sqrt{1 - \frac{\epsilon}{\omega_{01}}} |R\rangle \right), \quad (122)$$

$$|1\rangle = \frac{1}{\sqrt{2}} \left(\sqrt{1 - \frac{\epsilon}{\omega_{01}}} |L\rangle - \sqrt{1 + \frac{\epsilon}{\omega_{01}}} |R\rangle \right), \quad (123)$$

where $\omega_{01} = \sqrt{\epsilon^2 + \Delta^2}$. Approximating the localized flux states $|L\rangle$ and $|R\rangle$ as Gaussians centered in the minima of the double well, the relaxation rate T_1^{-1} and the pure dephasing rate T_ϕ^{-1} are given by

$$\frac{1}{T_1} \approx \left(\frac{\Delta}{\omega_{01}} \right)^2 |\mathbf{m} \cdot \Delta\boldsymbol{\varphi}|^2 \left(1 + \frac{S^2}{2} \right)^2 J(\omega_{01}) \coth \frac{\omega_{01}}{2k_B T}, \quad (124)$$

$$\frac{1}{T_\phi} \approx \left(\frac{\epsilon}{\omega_{01}} \right)^2 |\mathbf{m} \cdot \Delta\boldsymbol{\varphi}|^2 \left(1 + \frac{S^2}{2} \right)^2 \frac{J(\omega)}{\omega} \Big|_{\omega \rightarrow 0} 2k_B T, \quad (125)$$

where $S = \langle L|R\rangle$ is the overlap between the two Gaussians. The vector $\Delta\boldsymbol{\varphi}$ connects the two minima of the double well. These relations are valid in the Markov limit and at first order in Born approximation, where the system-bath interaction is considered only at first order. By inspection of the previous formula it is clear that a symmetric double well potential, for which $\epsilon = 0$, let the dephasing time to diverge. This is realized for a value of the external applied magnetic flux $\Phi_{\text{ext}} = \Phi_0/2$, being $\epsilon \propto (\Phi_{\text{ext}}/\Phi_0 - 1/2)$. Moreover for $\mathbf{m} \cdot \Delta\boldsymbol{\varphi} = 0$ the environment is decoupled from the system, and both the relaxation and dephasing time diverge.

In Ref. [96] an estimate of the leakage rate due to transition from the qubit states $k = 0, 1$ to higher energy levels $n = 2, 3, \dots$ outside the qubit subspace can be quantified from Eqs.(117) and (119),

$$\frac{1}{T_{L,k}} = 4 \sum_n |\langle n|\mathbf{m} \cdot \boldsymbol{\varphi}|k\rangle|^2 J(\omega_{kn}) \coth \frac{\omega_{kn}}{2k_B T}. \quad (126)$$

In the regime $\eta \gg \Delta, \delta, \epsilon$, where η is the energy splitting between the lowest two states $|L\rangle$ and $|R\rangle$ and the third energy level, and δ is the coupling between the qubit subspace and the next higher level, the dominant leakage occurs with rate

$$\frac{1}{T_L} \approx 4 \left(\frac{\delta}{\eta} \right)^2 |\mathbf{m} \cdot \Delta\boldsymbol{\varphi}|^2 J(\eta) \coth \frac{\eta}{2k_B T}, \quad (127)$$

and in the regime in which the two-level approximation is well defined, $\Delta \gg k_B T$, thermally activated leakage is strongly suppressed.

1.20.2 Thermal photon noise induced dephasing. Besides magnetic flux fluctuations, an important source of dephasing is represented by thermal photon noise in the read-out part of the circuit. To measure the state of the qubit a superconducting quantum interference device (SQUID) is coupled to the qubit via mutual inductance. When the SQUID is biased by a current that has a value smaller than the critical current, the SQUID acts just as an effective inductor, whose linear inductance depends on the qubit current state. The critical current at which the SQUID switch to a normal state can have two values $I_c^{(0)}$ and $I_c^{(1)}$, according to the two qubit possible current states. A bias current pulse of amplitude I_B , $I_c^{(0)} < I_B < I_c^{(1)}$, allows to discriminate the two qubit states. The read-out apparatus consisting of a dc-SQUID and a shunt capacitor C_s form a weakly damped harmonic oscillator of frequency ω_{ho} , that is detuned from the qubit frequency ω_q . The presence of n photons in the harmonic oscillator induces a shift in the qubit frequency, $\omega_{q,n} - \omega_{q,0} = n\delta\omega_0$, where the shift per photon depends on the effective qubit-oscillator coupling. Assuming that the pure dephasing time τ_ϕ is much larger than the inverse of the damping rate κ , $\tau_\phi \gg 1/\kappa$, thermally excited photons in the oscillator produce a dephasing [86, 101, 102]

$$\tau_\phi = \frac{\kappa}{\bar{n}(\bar{n} + 1)\delta\omega_0^2}, \quad (128)$$

where $\bar{n} = (\exp(\hbar\omega_{\text{ho}}/k_B T) - 1)^{-1}$ is the thermal average number of photon in the oscillator. A similar effect has been observed in an experimental work [87] in which a charge qubit is coupled to a superconducting waveguide resonator, slightly detuned from the qubit frequency. There, opposite to the case here described, the oscillator is driven and a shift and a broadening in the qubit resonance frequency appears, as a consequence of an ac-Stark shift and of photon shot noise.

The flux qubit of Ref. [102] has been engineered with four Josephson junction to ensure a symmetric qubit-SQUID coupling [103]. In the usual design of the Delft qubit [92], the two symmetric arms of the SQUID render the qubit immune to bias current I_B fluctuations. At zero dc bias, $I_B = 0$, a small fluctuating current caused by the finite impedance of the external controls is divided equally into two branches of the SQUID loop and no net current flows through the three-Josephson junctions of the qubit line. However, the double layer structure of the Josephson junctions, being an artefact of the shadow evaporation technique used to construct Josephson junctions, induces

asymmetry in the circuit. Using a fourth much larger Josephson junction, for which the Josephson energy can be usually neglected, symmetry in the double layer structure is restored and effects of fluctuations in the bias current are suppressed.

The qubit energy bias can be written as the sum of two contributions, $\epsilon = \eta + \lambda$, where $\eta = 2I_p(\Phi_{\text{ext}} - \Phi_0/2)$ (I_p is the qubit persistent current) is controlled by the external flux Φ_{ext} and $\lambda = 2I_p M J(I_B)/h$ which depends on I_B via the SQUID circulating current. This dependence has two crucial consequences: first the qubit bias point Φ_{ext}^* for which $\partial\omega_q/\partial\Phi_{\text{ext}} = 0$ results shifted by the measurement pulse. Therefore it is possible to operate the qubit at the flux-insensitive point, while keeping a difference in the expectation value of the current in the two qubit states, which is a crucial requirement for measuring the qubit state. Second a coupling between the qubit and the external harmonic oscillator, the so-called plasmon mode, arises, with an interaction Hamiltonian

$$\mathcal{H}_{\text{q-ho}} \propto [g_1(I_B)(a + a^\dagger) + g_2(I_B)(a + a^\dagger)^2]\sigma_z, \quad (129)$$

where $g_1(I_B) \propto (d\lambda/dI_B)$ and $g_2(I_B) \propto (d^2\lambda/dI_B^2)$ [101]. For a particular I_B^* that realizes $d\lambda/dI_B = 0$, it is possible to switch $g_1(I_B)$ off [102, 103].

Working at these optimal points, the qubit is immune from external flux and bias current fluctuations at first order, $\partial\omega_q/\partial\Phi_{\text{ext}}(\Phi_{\text{ext}}^*, I_B^*) = \partial\omega_q/\partial I_B(\Phi_{\text{ext}}^*, I_B^*) = 0$. The shift per photon of $\delta\omega_0$ is given, at second order perturbation theory in $\mathcal{H}_{\text{q-ho}}$ [101, 102], by

$$\delta\omega_0 = 4 \left[(g_1(I_B) \sin \theta)^2 \frac{\omega_q}{\omega_{\text{ho}}^2 - \omega_q^2} - g_2(I_B) \cos \theta \right], \quad (130)$$

where $\cos \theta = \epsilon/\omega_q$. For some value $\epsilon^*(I_B) < 0$ one obtains $\delta\omega_0 = 0$. In Ref. [102], via spectroscopy the authors demonstrated the existence of a line $\epsilon^*(I_B)$, that includes $I_B = I_B^*$ and $\epsilon = 0$, providing an optimal point with respect to bias current noise, flux noise, and photon noise. Measurements of the qubit spectral line shape at the optimal point showed, for the particular sample Ref. [102], a twin peak structure, which could arise from strong coupling to one microscopic fluctuator. An effective dephasing time $t_2 = 2/\pi(w_1 + w_2)$ is obtained by fitting the peaks with two Lorentzians of width w_1 and w_2 . Measurements of the spin-echo decay time T_{echo} , particularly indicated in case of relatively high frequency noise, as photon noise in the plasma mode that occurs at $\kappa \approx 130\text{MHz}$, gives at the optimal point $T_{\text{echo}} = 3.9\mu\text{s}$. By studying the variation of T_{echo} and t_2 as a function of ϵ , a sharp peak is found at $\epsilon = 0$ for $I_B = I_B^*$, while for $I_B = 0$ the peak shifts towards $\epsilon < 0$. The variation of the maximum in t_2 as a function of I_B show that the maximal coherence time

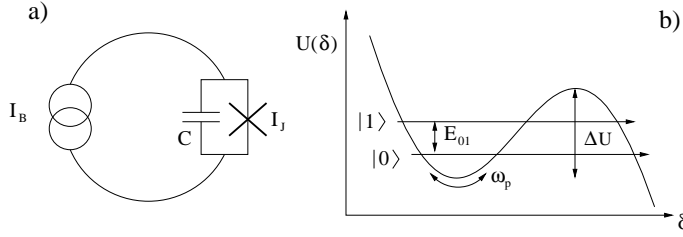


Figure 9. a) Schematic representation of the phase qubit circuit, constituted by a current-biased Josephson junction. b) Anharmonic potential $U(\delta)$ showing the two lowest energy states $|0\rangle$ and $|1\rangle$, separated by an energy splitting E_{01} . The plasma frequency ω_p is given by the local quadratic curvature of the potential at the bottom of the well, and ΔU is the potential barrier that separates the two energy levels in the well from a continuum of levels on the right side of the barrier.

is not obtained at $\epsilon = 0$, as it would be expected for flux or bias current noise. On the other hand, it fits with the line $\epsilon^*(I_B)$ for which $\delta\omega_0 = 0$, suggesting that thermally induced photon noise, rather than flux noise or bias current noise, is responsible for the qubit dephasing. For a temperature $T = 70\text{mK}$ and quality factor $Q = 150$, which yields a mean photon number $\bar{n} = 0.15$, the dephasing time τ_ϕ Eq. (128) closely matches the spin-echo measurements.

1.21 The superconducting phase qubit

The phase qubit works in a regime in which $E_J \gg E_C$ and the circuit consists of a loop with a single large Josephson junction, as shown in Fig. 9 (a). The circuit is biased with a current I typically driven close to the critical current I_0 of the junction. The Hamiltonian of the system is

$$H = \frac{\hat{Q}^2}{2C} - \frac{I_0\Phi_0}{2\pi} \cos \hat{\delta} - \frac{I\Phi_0}{2\pi} \hat{\delta} \quad (131)$$

where $\Phi_0/2\pi = \hbar/2e$ is the superconducting flux quantum. Charge and phase operators, \hat{Q} and $\hat{\delta}$, that correspond to the charge on the Josephson junction capacitance and the superconducting phase across the Josephson junction respectively, are conjugate variables that satisfy the canonical commutation rule $[\hat{\delta}, \hat{Q}] = 2ei$. For a large area junction $I_0\Phi_0/2\pi = E_J \gg E_C = e^2/2C$ the superconducting phase has a well defined value and quantum mechanical behavior can be observed. The Josephson inductance and the junction capacitance form an anharmonic ‘‘LC’’ resonator. The anharmonic potential as a function of the superconducting phase across the junction can be approximated by a cubic potential parametrized by the potential barrier $\Delta U(I) = (2\sqrt{2I_0\Phi_0/3\pi})[1 - I/I_0]^{3/2}$ and a classical plasma oscillation frequency at the bottom of the potential well $\omega_p(I) = 2^{1/4}(2\pi I_0/\Phi_0 C)^{1/2}[1 - I/I_0]^{1/4}$. The two

qubit states $|0\rangle$ and $|1\rangle$ are encoded in the two lowest quantum states in the potential well, and have energy splitting $E_{01} = \hbar\omega_p(1 - 5\hbar\omega_p/36\Delta U)$. Unlike in a flux or charge qubit, in a phase qubit the state ($|0\rangle$ or $|1\rangle$) is exclusively distinguished by the phase wavefunction, and not by any macroscopic quantity, such as current or charge. Transitions are driven by applying microwaves at frequency $\omega_{01} = E_{01}/\hbar$. For more details on the phase qubit we refer to Ref. [94].

Coherent control of the qubit is obtained through the bias current

$$I(t) = I_{\text{dc}} + I_{1/f}(t) + I_{\mu wc}(t) \cos(\omega_{01}t) + I_{\mu ws}(t) \sin(\omega_{01}t), \quad (132)$$

where $I_{1/f}$, $I_{\mu wc}$, and $I_{\mu ws}$ are varied in time slowly compared to $2\pi/\omega_{01}$. In the frame rotating with frequency ω_{01} , the qubit Hamiltonian is given by

$$H = \epsilon \frac{\Phi_0}{2\pi} I_{\mu wc}(t) \sigma_x + \epsilon \frac{\Phi_0}{2\pi} I_{\mu ws}(t) \sigma_y + \frac{1}{2} \frac{\partial E_{01}}{\partial I_{\text{dc}}} I_{1/f}(t) \sigma_z, \quad (133)$$

where $\epsilon = \sqrt{E_C/E_{01}}$, and $\sigma_{x,y,z}$ are the Pauli operators.

1.21.1 Decoherence of a phase qubit due to an arbitrary noise source.

Since the qubit is controlled by the bias current, noise in the bias current can represent a source of decoherence for the qubit. In Ref. [104] a physical picture of decoherence is presented for a phase qubit.

In a Bloch picture, the state of the qubit is represented by $|\psi\rangle = \cos(\theta/2)|0\rangle + e^{i\phi} \sin(\theta/2)|1\rangle$. Low frequency noise induces fluctuations in the longitudinal z component of the pseudo-spin representing the qubit that lead to dephasing of the qubit. The phase noise after time t is

$$\phi_n(t) = \frac{\partial \omega_{01}}{\partial I_{\text{dc}}} \int_0^t dt' I_n(t'), \quad (134)$$

and it arises from current noise $I_n(t)$. The magnitude of the phase noise is described by $\langle \phi_n^2(t) \rangle$, and it can be obtained through the noise spectral density $S_I(f)$,

$$\langle \phi_n^2(t) \rangle = \left(\frac{\partial \omega_{01}}{\partial I_{\text{dc}}} \right)^2 \int_0^{\omega_{01}/2\pi} df S_I(f) W_0(f), \quad (135)$$

where $S_I(f)$ is given by the Fourier transform of noise correlator $\langle I_n(t) I_n(0) \rangle = \int_0^\infty df S_I(f) \cos(2\pi ft)$, the spectral weight $W_0(f) = \sin^2(\pi ft)/(\pi f)^2$, and the integral on the frequency has been cutoff for frequency greater than $\omega_{01}/2\pi$.

This last assumption is justified since for those frequencies the noise current flows mainly through the junction capacitance, rather than the junction itself, thus not substantially affecting ω_{01} . The magnitude of noise is defined as the mean-square amplitude of the current noise at frequency f per 1 Hz bandwidth. For low frequency $f \leq 1/t$, $W_0(f)$ is rather constant, whereas it decreases as $1/f^2$ at higher frequencies. As a consequence, phase noise affects the qubit dynamics only at low frequencies for most noise sources. For constant (white) noise S_I^0 , one has

$$\langle \phi_n^2(t) \rangle = \left(\frac{\partial \omega_{01}}{\partial I_{\text{dc}}} \right)^2 \frac{S_I^0 t}{2}. \quad (136)$$

At higher frequencies close to ω_{01} , noise induces transitions between the two qubit states $|0\rangle$ and $|1\rangle$. The current that controls these transitions is given by $I_{\mu wc}(t) \cos(\omega_{01}t) + I_{\mu vs}(t) \sin(\omega_{01}t)$, and mixing from noise around frequency ω_{01} can be understood as low frequency noise in $I_{\mu wc}(t)$ and $I_{\mu vs}(t)$. Random fluctuations along the transverse x and y components of the qubit induce transitions between the qubit states. For constant spectral density around ω_{01} given by $2S_I(\omega_{01}/2\pi)$, an application of the previous results gives

$$\langle \theta_x^2(t) \rangle = \langle \theta_y^2(t) \rangle = \frac{E_C}{E_{01}} \left(\frac{\Phi_0}{2\pi} \right)^2 S_I(\omega_{01}/2\pi)t. \quad (137)$$

The random angles $\chi = \phi, \theta_x$ and θ_y are assumed to be Gaussian distributed, with zero mean and mean squared noise $\langle \chi^2 \rangle$ previously calculated, $dp(\chi)/d\chi = \exp(-\chi^2/2\langle \chi^2 \rangle)/\sqrt{2\pi\langle \chi^2 \rangle}$.

If the qubit is initially in the ground state, that is when it is parallel to the z direction in the Bloch sphere, when the noise is small, it is immune to phase noise at low frequency. However, transverse noise around frequency ω_{01} can induce transitions in between the qubit states. The probability p_0 to be in the state $|0\rangle$ is given in the Bloch picture by $\cos^2(\theta/2) \simeq \cos^2[\sqrt{\theta_x^2 + \theta_y^2}/2]$. With the values previously obtained for the mean-square noise, averaging over the Gaussian distribution gives

$$p_0 = \frac{1}{2} \left(1 + e^{-t/T_1} \right), \quad \frac{1}{T_1} = \frac{E_C}{E_{01}} \left(\frac{\Phi_0}{2\pi} \right)^2 S_I(\omega_{01}/2\pi). \quad (138)$$

The rate $1/T_1$ describes absorption and emission rate for the stimulated transitions $0 \rightarrow 1$ and $1 \rightarrow 0$. Since low frequency noise cannot add energy $\hbar\omega_{01}$, there is no contribution from phase noise.

Effects of noise on a superposition state can be understood within a ‘‘Ram-

sey fringe” picture. Through a $\pi/2$ pulse the qubit is rotated from the ground state $|0\rangle$ to the state $(|0\rangle + |1\rangle)/\sqrt{2}$, that points in the x direction in the Bloch sphere, and left evolving for a time t , after which a subsequent $\pi/2$ pulse is performed and the qubit state is finally measured. During the evolution between the two $\pi/2$ pulses, the state of the qubit can change due to noise in ϕ and θ_y , therefore, both phase and stimulated transitions noise affect the qubit dynamics. In this case the total decoherence rate is given by the Korringa relation [9] $1/T_2 = 1/T_\phi + 1/2T_1$, where $1/T_\phi$ is directly extracted from Eq. (136) $1/T_\phi = (\partial\omega_{01}/\partial I_c)^2 S_I^0/4$.

1.22 Decoherence due to $1/f$ noise

Much effort has been spent recently to understand how noise at low frequencies affects the dynamics of superconducting qubit, both from a theoretical and an experimental point of view. In particular, signatures of non-Markovian dynamics are believed to be due to $1/f$ noise. Both charge and flux $1/f$ noise contribute to decoherence, the former affecting mostly the dynamics of superconducting qubits based on the charge degrees of freedom, and the latter affecting flux and phase qubits. Here we concentrate only on $1/f$ flux noise, and refer to the literature for the case of $1/f$ charge noise [105, 106].

1.22.1 Model for $1/f$ flux noise in SQUIDS. The origin of $1/f$ flux noise in low- T_c devices has not yet been completely understood. Critical-current fluctuations in Josephson junctions are believed to arise from trapping and release of electrons in traps in the tunnel barriers. In Ref. [107], a model for $1/f$ noise in low- T_c devices is proposed, based on the assumptions that it arises from thermally activated hopping of unpaired electrons on and off defects. The spin of the electron is locked in direction while the electron is trapped, and the directions are randomly change from trap to trap. Uncorrelated changes of these spin directions give rise to random telegraph signals that produce a $1/f$ power spectrum. The electron is assumed to occupy the low-energy spin direction during the entire time it resides on the defect. For zero magnetic field \mathbf{B} , transitions between the two degenerate Kramers’ doublet are strongly suppressed, implying that direct phonon scattering is forbidden. On the other hand, the magnetic field is not strictly zero, and fluctuating dipole fields can arise from neighboring defects.

The magnetic moment of a defect $\hat{\mathbf{M}} = \mu_B(\hat{\mathbf{L}} + 2\hat{\mathbf{S}})$ can be locked as a consequence of spin-orbit coupling, that makes it stable with respect to these

weak fluctuations. The locking effect can be modeled by the Hamiltonian

$$H = \sum_{i=x,y,z} V_i |p_i\rangle \langle p_i| + \lambda \hat{\mathbf{L}} \cdot \hat{\mathbf{S}} + \mu_B \mathbf{B} \cdot (\hat{\mathbf{L}} + 2\hat{\mathbf{S}}). \quad (139)$$

The unpaired electron occupies a p orbital, and $V_{x,y,z}$ are the matrix elements of the crystal-field potential. The spin-orbit coupling constant, depending on the different kind of defects, can vary in magnitude within a large range of values, but for defects involving atomic weights near that of Si, $|\lambda| \approx 300$ K. The crystal-field $V_{x,y,z}$ can be at most ≈ 2000 K. In defects for which $\lambda < 0$, \mathbf{L} and \mathbf{S} are parallel and \mathbf{M} is large, while for defects for which $\lambda > 0$ \mathbf{L} and \mathbf{S} are antiparallel, and \mathbf{M} is close to zero. Therefore, the $\lambda < 0$ defects are expected to be most important for flux noise.

A random distribution of defects over the substrate is assumed, and the flux noise coupled into a SQUID by a spatially random distribution of electron spins, whose orientations fluctuate, is calculated. The magnetic moment is represented by a small current loop that couples to the SQUID loop by a mutual inductance $M(x, y)$. The SQUID loop is schematized like a square frame of inner and outer dimensions of $2d$ and $2D$, and thickness $W = D - d$, lying in the plane $z = 1 \mu\text{m}$. The current loop can lie in the $z = 0 \mu\text{m}$ plane, resulting in a perpendicular moment, or in the x or y plane centered at $z = 0$, resulting in a in-plane moment. The small loop current has an effective area $A = (0.1 \mu\text{m})^2$, and a current i flows in it, such that $Ai = \mu_B$, with flux per Bohr magneton given by $\Phi_s/\mu_B = M(x, y)/A$. Perpendicular and in-plane flux per Bohr magneton show a qualitative opposite behavior as function of the position in the SQUID loop plane, the former peaking on the edges of the superconductor, and the latter peaking at the midpoint of the superconductor, both falling off away from these points. The total mean square normalized flux noise coupled to the SQUID is given by

$$\langle (\delta\Phi_s)^2 \rangle = 8n\mu_B^2 \int_0^{L+D} dx \int_0^x dy \frac{M^2(x, y)}{A^2}, \quad (140)$$

where n is the areal density of defects, and the integral over the plane is cutoff a distance L away from the SQUID loop. The mean square noise is given by $\langle (\delta\Phi_{\text{st}})^2 \rangle = [\langle (\delta\Phi_{\text{si},x})^2 \rangle + \langle (\delta\Phi_{\text{si},y})^2 \rangle + \langle (\delta\Phi_{\text{sp}})^2 \rangle]/3$, and the spectral density $S_\Phi(f) = \alpha/f$ is extracted by $\langle (\delta\Phi_{\text{st}})^2 \rangle = \alpha \int_{f_1}^{f_2} df/f = \alpha \ln(f_2/f_1)$, and, for $f_2/f_1 \approx 10^{13}$,

$$S_\Phi(f)/\Phi_0^2 \approx \langle (\delta\Phi_s/\Phi_0)^2 \rangle / 30f. \quad (141)$$

Noise levels in agreement with the observations are obtained for $n \approx$

10^{17} m^{-2} . However, they strongly vary with the geometry of the the SQUID and the tunnel barriers, and with the fabrication details.

1.22.2 Decoherence of flux qubits due to $1/f$ noise. Recently experiments [108,109] have reported the behavior of the echo signal in flux qubits at various bias conditions. The energy splitting depends on the applied external magnetic flux, and thus it is sensitive to flux noise. As a result they found that the at the optimal point, where the energy splitting is insensitive at first order to magnetic flux fluctuations, the coherence time is limited by energy relaxation processes, T_1 , and the dephasing of the flux qubit is mostly determined by the high-frequency noise $S_\Phi(\omega \approx \Delta/\hbar)$.

In a Markovian approximation the energy relaxation contributes to the dephasing process via $1/T_2^{\text{echo}} = 1/2T_1 + \Gamma_\varphi$, where Γ_φ is the pure dephasing rate. For dephasing dominated by magnetic flux noise with a smooth spectrum near $\omega = 0$, the pure dephasing rate is given by $\Gamma_\varphi^\Phi \approx (\partial\Delta E/\partial\Phi_{\text{ext}})^2 S(\omega = 0)$, where $\Delta E = \sqrt{\epsilon(\Phi_{\text{ext}})^2 + \Delta^2}$. Taking into account the fact that, from their experimental data, the relaxation time T_1 is almost independent on the external applied magnetic flux, and that close to the optimal point the $\partial\Delta E/\partial\Phi_{\text{ext}} \propto \Phi_{\text{ext}}$, a parabolic behavior of $1/T_2^{\text{echo}}$ is expected in this region. On the other hand, away from the optimal point, they observed a linear increasing of $1/T_2^{\text{echo}}$ with respect of the applied external magnetic flux. Therefore, the experimental data cannot be explained within the framework of Bloch-Redfield decoherence theory, in which the assumption of short time correlated noise (white noise around $\omega = 0$) holds.

The experimental observations can be explained with the presence of $1/f$ flux noise. In Refs. [108,109], in order to separate the contribution to dephasing due to direct transitions between energy levels, the echo signal is expressed as $\rho(t) = e^{-t/2T_1} \rho_{\text{echo}}(t)$, with $\rho(t) = \langle \sigma_z \rangle$. In this case the expectation value of σ_z is given by a non-exponential decay curve, and at the end of the echo sequence

$$\rho_{\text{echo}}(t) = \left\langle \exp \left\{ -iv_\Phi \left[\int_0^{t/2} \Phi(\tau) d\tau - \int_{t/2}^t \Phi(\tau) d\tau \right] \right\} \right\rangle, \quad (142)$$

where $v_\Phi = (\Phi_0/\hbar)\partial\Delta E/\partial\Phi_{\text{ext}}$. Assuming Gaussian statistics of the fluctuations of the external flux, the decoherence rate can be expressed through the noise spectral function, $S_\Phi(\omega) = (1/\pi) \int_0^\infty dt \cos \omega t \langle \Phi(t)\Phi(0) \rangle$,

$$\rho(t) = \exp \left[-\frac{t^2 v_\Phi^2}{2} \int_{-\infty}^\infty S_\Phi(\omega) \frac{\sin^4(\omega t/4)}{(\omega t/4)^2} \right] \quad (143)$$

For a $1/f$ spectrum $S_\Phi = A_\Phi/\omega$ one obtains

$$\rho_{\text{echo}}(t) = \exp [-(\Gamma_\varphi^\Phi t)^2], \quad \Gamma_\varphi^\Phi \equiv |v_\Phi| \sqrt{A_\Phi \ln 2}. \quad (144)$$

In Ref. [110], motivated by the experimental results of Refs. [108, 109], a theoretical analysis of the dephasing due to $1/f$ noise in flux qubits has been presented. The problem is described by choosing spin-fluctuators as source of low-frequency noise. Random switching of a fluctuator between its two metastable states gives rise to a random telegraph noise. Transitions in fluctuators with energy splitting larger than the temperature are strongly suppressed and only fluctuators whose energy splitting is smaller than the temperature contribute to the qubit dephasing. For a random telegraph process, $\xi(t)$, in which a switching between the values $\pm 1/2$ takes place at random times, the probability to make n transition in a certain amount of time τ is Poisson distributed. As a consequence, the time correlation function $\langle \xi(t)\xi(0) \rangle = e^{-|\gamma|t}/4$ decays exponentially, with $|\gamma|$ given by the rate of the transition between the to states of the fluctuator. The contribution to the noise spectrum of a random telegraph process, given by the Fourier transform of the correlation function, is a Lorentzian, $\gamma/4\pi(\omega^2 + \gamma^2)$. The effects of many uncorrelated fluctuators coupled to the qubit via constants v_i simply add. Considering a large number of effective spin-fluctuators and assuming no correlations between couplings v_i and switching rates γ_i , the noise spectral function is give by

$$S(\omega) = \frac{\langle v^2 \rangle}{4\pi} \int \frac{\gamma \mathcal{P}_\gamma(\gamma)}{\gamma^2 + \omega^2} d\gamma. \quad (145)$$

The distribution $\mathcal{P}_\gamma(\gamma)$ depends on the details of the interaction between the fluctuators and the qubit. Following [110, 111], $\mathcal{P}_\gamma(\gamma) \sim (A/\gamma)\Theta(\gamma - \gamma_0)$, where γ_0 represent the maximal relaxation rate for fluctuators with a given energy splitting E , and A gives the amplitude of the $1/f$ noise. It follows for the noise spectral function

$$S(\omega) = \frac{A}{\omega} \times \begin{cases} 1 & , \omega \ll \gamma_0 \\ 2\gamma_0/\pi\omega & , \omega \gg \gamma_0 \end{cases}. \quad (146)$$

The spin-fluctuator model reproduces $1/f$ noise power spectrum for $\omega \ll \gamma_0$, but it predicts a crossover from a ω^{-1} to ω^{-2} behavior, consequence of the assumption of a maximal switching rate γ_0 . Expressing the fluctuation of the magnetic flux as sum of the contributions of the independent fluctuators $\Phi(t) = \sum_i b_i \xi_i(t)$, in a Gaussian approximation, substitution of Eq. (146) in Eq. (143)

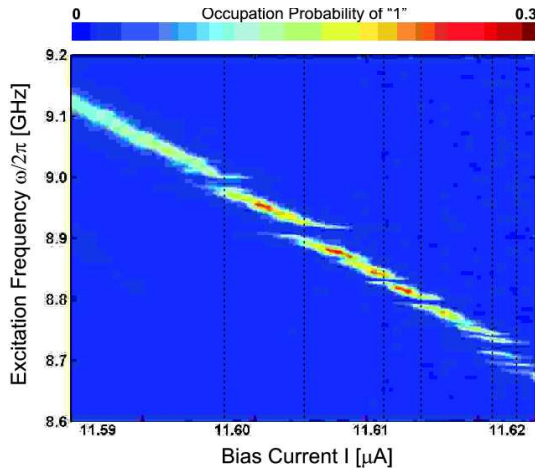


Figure 10. Measured probability of state “1” versus microwave excitation frequency $\omega/2\pi$ and bias current I for a fixed microwave power for a phase qubit, obtained from Ref. [112]. Dotted vertical line indicate spurious resonators. (With permission from the Authors).

leads to

$$\mathcal{K}_g = -\ln \rho = \langle v_\Phi^2 b^2 \rangle A t^2 \times \begin{cases} \gamma_0 t / 6, & \gamma_0 t \ll 1, \\ \ln 2, & \gamma_0 t \gg 1. \end{cases} \quad (147)$$

Therefore the echo signal is expected to decay in a Gaussian way at long times $t \gg \gamma_0^{-1}$, while at short times $t \ll \gamma_0^{-1}$ a faster decay is expected, $\mathcal{K}_g \propto t^3$.

Using the method of stochastic differential equations (see [110] and references therein), an estimate for the non-Gaussian case provides for the logarithm of the echo signal \mathcal{K}_{sf} [110]

$$\mathcal{K}_{\text{sf}} \approx \begin{cases} \gamma_0 A \bar{v}^2 t^3 / 6, & t \ll \gamma_0^{-1} \\ \ln 2 A \bar{v}^2 t^2, & \gamma_0^{-1} \ll t \ll \bar{v}^{-1} \\ \alpha \bar{v} A t, & \bar{v}^{-1} \ll t, \end{cases} \quad (148)$$

where \bar{v} is the center of a sharp peaked distribution of the couplings between the fluctuators and the qubit, and $\alpha \approx 6$. A new decaying behavior arise in the case of large time $t \gg \bar{v}^{-1}$, that drastically differs from the predictions of Gaussian statistically distributed magnetic flux fluctuations. The reason laying in the fact at short time only fast “fast” fluctuators contribute to the dephasing, giving rise, for $v \ll \gamma$, to Gaussian decay, while at long time non-Gaussian behavior appears.

1.22.3 $1/f$ noise in superconducting phase qubit. In this section we review the latest results on decoherence of superconducting phase qubits [93,94]. Recent experiments [112,113] have pointed out that a dominant source of decoherence for the phase qubit is represented by low frequency $1/f$ noise, that is believed to arise from two level systems (TLS) in the insulating barrier of the tunnel junction as well as in the dielectric material surrounding the circuit. In Fig. 10 a measurement of the transition frequency ω_{01} between the two qubit state, as a function of the bias current I and the microwave excitation frequency $\omega/2\pi$, shows a qubit line in which a number of spurious resonators appear, characteristic of energy-level repulsion predicted for coupled two-state systems. Near the resonators, the Rabi oscillations show beating, loss and recovery of the oscillations with time, and rapid decrease of coherence amplitude. The beating behavior is consistent with the interaction of a qubit with another two-level system, but not with harmonic oscillator modes in the read-out SQUID. Moreover, each qubit has its own set of resonator frequencies and strength, indicating that the TLS have a microscopic origin.

A new method to measure $1/f$ noise in Josephson junction qubits has been recently presented in [114]. It uses the resonant response of the qubit to directly measure the spectrum of the low-frequency noise, and allows to distinguish between flux and critical-current fluctuations by comparison of the noise taken at positive and negative bias. Remarkably it can yield low-frequency spectra below 1 Hz. Dephasing is produced by low-frequency fluctuations in the qubit energy, which in this study are believed to arise from magnetic flux noise in the qubit loop, with a spectral density that scales inversely with frequency, $1/f$. It turns out that the flux-like noise predominates over critical-current noise.

The possibility that flux noise is due to TLS defects in the native oxides of the superconductive film, as proposed in [107], is examined in Ref. [114]. Following [115] for a standard TLS model [116] a theoretical estimation of the flux noise spectral density, for a realistic geometry of the circuit loop, gives $S_{\Phi}(1 \text{ Hz}) \approx 10^{-3}(\mu\Phi_0)^2/\text{Hz}$, about 4 orders of magnitude smaller than the measured flux noise. This estimate is based on the assumption that TLS fluctuations randomizes the defect magnetic moment; assumption highly questionable because TLS defects in typical oxides are not considered to be magnetic.

References

- [1] N. F. Ramsey, A molecular beam resonance method with separated oscillating fields, Phys. Rev. **78**, 695 - 699 (1950)
- [2] S. Nakajima, On quantum theory of transport phenomena, Progr. Theor. Phys. **20**, 948 (1958)
- [3] R. Zwanzig, J. Chem. Phys. **33**, 1338 (1960); R. Zwanzig, in: *Lectures in Theoretical Physics* (Boulder), Vol. 3, ed. by W. E. Brittin, B. W. Downs, and J. Downs (Interscience, New York, 1961)
- [4] A. G. Redfield, Adv. Magn. Reson. **1**, 1 (1965)

- [5] K. Blum, *Density matrix theory and applications* (Plenum Press, 1981)
- [6] C. P. Slichter, *Principles of magnetic resonance* (North-Holland, Amsterdam, 1987)
- [7] G. Lindblad, On the generators of quantum dynamical semigroups, *Commun. Math. Phys.* **48**, 119 (1976)
- [8] A. G. Redfield, *IBM J. Res. Dev.* **1**, 19 (1957)
- [9] A. Abragam, *The principles of nuclear magnetism* (Clarendon Press, Oxford, 1961)
- [10] A. O. Caldeira and A. J. Leggett, Quantum tunneling in a dissipative system *Ann. Phys. (San Diego)* **149**, 374 (1983)
- [11] A. J. Leggett, S. Chakravarty, A. T. Dorsey, M. P. A. Fisher, A. Garg, W. Zwerger, Dynamics of the dissipative two-state system, *Rev. Mod. Phys.* **59**, 1 - 85 (1987)
- [12] U. Weiss, *Quantum dissipative systems*, (World Scientific Publishing, London, 1999)
- [13] D. P. DiVincenzo and D. Loss, Rigorous Born approximation and beyond for the spin-boson model, *Phys. Rev. B* **71**, 035318 (2005)
- [14] D. P. DiVincenzo, and D. Loss Exact Born approximation for the spin-boson model, arxiv:cond-mat/0304118 v2 (2003)
- [15] D. P. DiVincenzo, Quantum computation, *Science* **270**, 255 (1995)
- [16] D. Loss and D. P. DiVincenzo, Quantum computation with quantum dots, *Phys. Rev. A* **57**, 120 (1998)
- [17] J. R. Petta, J. M. Taylor, A. C. Johnson, A. Yacoby, M. D. Lukin, C. M. Marcus, M. P. Hanson, A. C. Gossard, Dynamic nuclear polarization with single electron spins, arXiv:0709.0920
- [18] Alexander V. Khaetskii and Yuli V. Nazarov, Spin relaxation in semiconductor quantum dots, *Phys. Rev. B* **61**(19), 12639 (2000)
- [19] Alexander V. Khaetskii and Yuli V. Nazarov, Spin-flip transitions between Zeeman sublevels in semiconductor quantum dots, *Phys. Rev. B* **64**(19), 125316 (2001)
- [20] T. Fujisawa, T. H. Oosterkamp, W. G. van der Wiel, B. W. Broer, R. Aguado, S. Tarucha, L. P. Kouwenhoven, Spontaneous emission spectrum in double quantum dot devices, *Science* **282**, 932 (1998)
- [21] S. Amasha, K. MacLean, Iuliana P. Radu, D. M. Zumbuhl, M. A. Kastner, M. P. Hanson, A. C. Gossard, Electrical control of spin relaxation in a quantum dot, arXiv:0707.1656, (2007)
- [22] G. Burkard, D. Loss, and D. P. DiVincenzo, Coupled quantum dots as quantum gates, *Phys. Rev. B* **59**, 2070 (1999)
- [23] W. A. Coish, E. A. Yuzbashyan, B. L. Altshuler, and Daniel Loss, Quantum vs. classical hyperfine-induced dynamics in a quantum dot, *J. Appl. Phys.* **101**, 081715 (2007)
- [24] D. Paget, G. Lampel, B. Sapoval, and V. I. Safarov, Low field electron-nuclear spin coupling in gallium arsenide under optical pumping conditions, *Phys. Rev. B* **15**, 7580 (1977)
- [25] I. A. Merkulov, A. L. Efros, J. Rosen, Electron spin relaxation by nuclei by semiconductor quantum dots, *Phys. Rev. B* **65**, 205309 (2002)
- [26] A. V. Khaetskii, D. Loss, L. Glazman, Electron spin decoherence in quantum dots due to interaction with nuclei, *Phys. Rev. Lett.* **88**, 186802 (2002)
- [27] A. V. Khaetskii, D. Loss, L. Glazman, Electron spin evolution induced by interaction with nuclei in a quantum dot, *Phys. Rev. B* **67**, 195329 (2003)
- [28] W. A. Coish, D. Loss, Hyperfine interaction in quantum dot: Non-Markovian electron spin dynamics, *Phys. Rev. B* **70**, 195340 (2004)
- [29] J. R. Petta, A. C. Johnson, J. M. Taylor, E. A. Laird, A. Yacoby, M. D. Lukin, C. M. Marcus, M. P. Hanson, and A. C. Gossard, Coherent manipulation of coupled electron spins in semiconductor quantum dots, *Science* **309**, 2180 (2005)
- [30] F. H. L. Koppens, D. Klauser, W. A. Coish, K. C. Nowack, L. P. Kouwenhoven, D. Loss, and L. M. K. Vandersypen, Universal phase shift and nonexponential decay of driven single-spin oscillations, *Phys. Rev. Lett.* **99**, 106803 (2007)
- [31] D. Klauser, W. A. Coish, and D. Loss, Nuclear spin state narrowing via gate-controlled Rabi oscillations in a double quantum dot, *Phys. Rev. B* **74**, 205302 (2006)
- [32] D. Stepanenko, G. Burkard, G. Giedke, and A. Imamoglu, Enhancement of electron spin coherence by optical preparation of nuclear spin, *Phys. Rev. Lett.* **96**, 136401 (2006)
- [33] K. Ono and S. Tarucha, Nuclear-spin-induced oscillatory current in spin-blockaded quantum dots, *Phys. Rev. Lett.* **92**, 256803 (2004)
- [34] F. H. L. Koppens, C. Buizert, K. J. Tielrooij, I. T. Vink, K. C. Nowack, T. Meunier, L. P. Kouwenhoven, L. M. K. Vandersypen, Driven coherent oscillations of a single electron spin in a quantum dot, *Nature (London)* **442**, 766 (2006)
- [35] W. A. Coish and Daniel Loss, Single-triplet decoherence due to nuclear spins in a double quantum dot, *Phys. Rev. B* **72**, 125337 (2005)

- [36] E. A. Laird, J. R. Petta, A. C. Johnson, C. M. Marcus, A. Yacoby, M. P. Hanson, and A. C. Gossard, Effect of exchange interaction on spin dephasing in a double quantum dot, *Phys. Rev. Lett.* **97**, 056801 (2006)
- [37] G. Giedke, J. M. Taylor, D. D'Alessandro, M. D. Lukin, and A. Imamoglu, Quantum measurement of a mesoscopic spin ensemble, *Phys. Rev. A* **74**, 032316 (2006)
- [38] W. A. Coish, J. Fischer, and D. Loss, Exponential decay in a spin bath, arXiv:0710.3762 2007
- [39] J. J. Sakurai, *Advanced quantum mechanics*, (Addison-Wesley, 1967)
- [40] G. Dresselhaus, Spin-orbit coupling effects in zinc blende structures, *Phys. Rev.* **100**, 580 (1955)
- [41] M. I. Dyakonov and V. Yu. Kachorovskii, Spin relaxation of two-dimensional electrons in non-centrosymmetric semiconductors, *Sov. Phys. Semicond.* **20**, 110 (1986)
- [42] M. I. Dyakonov and V. I. Perel, Spin orientation of electrons associated with interband absorption of light in semiconductors, *Sov. Phys. JETP* **33**, 1053 (1971)
- [43] E. I. Rashba, Properties of semiconductors with an extremum loop .I. Cyclotron and combi-national resonance in a magnetic field perpendicular to the plane of the loop, *Sov. Phys. Solid State* **2**, 1109 (1960)
- [44] Yu. A. Bychkov and E. I. Rashba, Properties of a 2D electro-gas with lifted spectral degeneracy, *JETP Lett.* **39**, 78 (1984)
- [45] G. E. Pikus and A. N. Tikov, *Optical orientation* (North-Holland, Amsterdam, 1984), p. 73
- [46] L. M. Roth, *g-Factor and Donor Spin-Lattice Relaxation for Electrons in Germanium and Silicon*, *Phys. Rev.* **118**, 1534 (1960)
- [47] V. I. Fal'ko, B. L. Altshuler, and O. Tsyplatyev, Anisotropy of spin splitting and spin relaxation in lateral quantum dots, *Phys. Rev. Lett.* **95**, 076603 (2005)
- [48] T. Meunier, I. T. Vink, L. H. Willems van Beveren, K-J. Tielrooij, R. Hanson, F. H. L. Koppens, H. P. Tranitz, W. Wegscheider, L. P. Kouwenhoven, and L. M. K. Vandersypen, Experimental Signature of Phonon-Mediated Spin Relaxation in a Two-Electron Quantum Dot, *Phys. Rev. Lett.* **98**, 126601 (2007)
- [49] D. Rugar, R. Budakian, H. J. Mamin, and B. W. Chui, Single spin detection by magnetic resonance force microscopy, *Nature (London)* **430**, 329 (2004)
- [50] J. M. Elzerman, R. Hanson, L. H. Willems van Beveren, B. Witkamp, L. M. K. Vandersypen, L. P. Kouwenhoven, Single-shot read-out of an individual electron spin in a quantum dot, *Nature (London)* **430**, 431 (2004)
- [51] M. Kroutvar, Yann Ducommun, Dominik Heiss, Max Bichler, Dieter Schuh, Gerhard Abstreiter, Jonathan J. Finley, Optically programmable electron spin memory using semiconductor quantum dots, *Nature (London)* **432**, 81 (2004)
- [52] D. V. Bulaev and D. Loss, Spin relaxation in quantum dots: Rashba versus Dresselhaus spin-orbit coupling, *Phys. Rev. B* **71**, 205324 (2005)
- [53] P. Stano and J. Fabian, Spin-orbit effects in single-electron states in coupled quantum dots, *Phys. Rev. B* **72**, 155410 (2005)
- [54] P. Stano and J. Fabian, Theory of phonon-induced spin relaxation in laterally coupled quantum dots, *Phys. Rev. Lett.* **96**, 186602 (2006)
- [55] V. N. Golovach, A. Khaetskii, and D. Loss, Phonon-induced decay of the electron spin in quantum dots, *Phys. Rev. Lett.* **93**, 016601 (2004)
- [56] P. San-Jose, G. Zarand, A. Shnirman, and G. Schön, Geometrical spin dephasing in quantum dots, *Phys. Rev. Lett.* **97**, 076803 (2006)
- [57] Al. L. Efros and M. Rosen, Quantum size level structure of narrow-gap semiconductor nanocrystals: Effect of band coupling, *Phys. Rev. B* **58**, 7120 (1998)
- [58] L. M. Woods, T. L. Reinecke, and R. Kotlyar Hole spin relaxation in quantum dots, *Phys. Rev. B* **69**, 125330 (2004)
- [59] C. Lü, J. L. Cheng, and M. W. Wu, Hole spin relaxation in semiconductor quantum dots, *Phys. Rev. B* **71**, 075308 (2005)
- [60] J. M. Luttinger and W. Kohn, Motion of electrons and holes in perturbed periodic fields, *Phys. Rev.* **97**, 869 (1955)
- [61] J. M. Luttinger Quatum theory of cyclotron resonance in semiconductors: General theory, *Phys. Rev.* **102**, 1030 (1956)
- [62] R. Winkler, Rashba spin splitting in two-dimensional electron and hole systems, *Phys. Rev. B* **62**, 4245 (2000)
- [63] R. Winkler, H. Noh, E. Tutuc, and M. Shayegan, Anomalous Rashba spin splitting in two-dimensional hole systems, *Phys. Rev. B* **65**, 155303 (2002)
- [64] D. V. Bulaev and D. Loss, Spin relaxation and decoherence of holes in quantum dots, *Phys. Rev. Lett.* **95**, 076805 (2005)

- [65] H. W. van Kesteren, E. C. Cosman, W. A. J. A. van der Poel, and C. T. Foxon, Fine structure of excitons in type-II GaAs/AlAs quantum wells, *Phys. Rev. B* **41**, 5283 (1990)
- [66] B. P. Zakharchenya and F. Meier, *Optical Orientation*, (North-Holland, Amsterdam, 1984)
- [67] D. V. Bulaev and D. Loss, Electric dipole spin resonance for holes in quantum dots, *Phys. Rev. Lett.* **98**, 097202 (2007)
- [68] D. Heiss, S. Schaeck, H. Huebel, M. Bichler, G. Abstreiter, J. J. Finley, D. V. Bulaev, and D. Loss, Observation of extremely slow hole spin relayation in self-assembled quantum dots, <http://arxiv.org/abs/0705.1466> (2007)
- [69] N. G. Ganichev, V. A. Margulis, and A. V. Shorokhov, Photoconductance of quantum wires in a magnetic field, *Phys. Rev. B* **69**, 113312 (2004)
- [70] V. Fock, Bemerkung zur Quantelung des harmonischen Oszillators im Magnetfeld, *Z. Phys.* **47**, 446-448 (1928)
- [71] C. G. Darwin, The diamagnetism of free electron, *Proc. Cambridge Phylos. Soc.* **27**, 86-90 (19300)
- [72] S. D. Ganichev, V. V. Bel'kov, L. E. Golub, E. L. Ivchenko, Petra Schneider, S. Giglberger, J. Eroms, J. De Boeck, G. Borghs, W. Wegscheider, D. Weiss, and W. Prettl, Experimental Separation of Rashba and Dresselhaus Spin Splittings in Semiconductor Quantum Wells, *Phys. Rev. Lett.* **92**, 256601 (2004)
- [73] F. H. L. Koppens, C. Buizert, K. J. Tielrooij, I. T. Vink, K. C. Nowack, T. Meunier, L.P. Kouwenhoven, and L. M. K. Vandersypen, Driven coherent oscillations of a single electron spin in a quantum dot, *Nature* **442**, 766 (2006)
- [74] R. Meisels, Electron spin resonance and related phenomena of low-dimensional electronic systems in III V compounds, *Semicond. Sci. Technol.* **20**, R1 (2005)
- [75] A. Abragam, *The principles of nuclear magnetism*, (Plenum, New York, 1996)
- [76] M. H. Devoret, Quantum fluctuations in electrical circuits, (S. Reynaud, E. Giacobino and J. Zinn-Justin, eds., 1997, Elsevier Science)
- [77] Y. Makhlin, G. Schön, and A. Shnirman, Quantum-state engineering with Josephson-junction devices, *Rev. Mod. Phys.* **73**, 357 (2001)
- [78] M. H. Devoret, A. Wallraff, J. M. Martinis, Superconducting qubits: a short review, [arXiv:cond-mat/0411174](http://arxiv.org/abs/cond-mat/0411174)
- [79] D. V. Averin, Adiabatic quantum computation with Cooper pairs, *Solid State Commun.* **105**, 659 (1998)
- [80] Y. Makhlin, Gerd Schön, Alexander Shnirman, Josephson-junction qubits with controlled couplings, *Nature* **398**, 305-307 (1999)
- [81] Y. Nakamura, Yu. A. Pashkin, J. S. Tsai, Coherent control of macroscopic quantum states in a single-Cooper-pair box, *Nature* **398**, 786-788 (1999)
- [82] Yu. A. Pashkin, T. Yamamoto, O. Astafiev, Y. Nakamura, D. V. Averin, J. S. Tsai, Quantum oscillations in two coupled charge qubits *Nature* **421**, 823-826 (2003)
- [83] A. Shnirman, G. Schön, and Z. Hermon, Quantum Manipulations of Small Josephson Junctions, *Phys. Rev. Lett.* **79**, 2371 - 2374 (1997)
- [84] D. Vion, A. Aassime, A. Cottet, P. Joyez, H. Pothier, C. Urbina, D. Esteve, and M. H. Devoret, Manipulating the Quantum State of an Electrical Circuit, *Science* **296**, 886 (2002)
- [85] A. Wallraff, D. I. Schuster, A. Blais, L. Frunzio, R.-S. Huang, J. Majer, S. Kumar, S. M. Girvin, R. J. Schoelkopf, Strong coupling of a single photon to a superconducting qubit using circuit quantum electrodynamics, *Nature* **431**, 162-167 (2004)
- [86] A. Blais, R.-S. Huang, A. Wallraff, S. M. Girvin, and R. J. Schoelkopf, Cavity quantum electrodynamics for superconducting electrical circuits: An architecture for quantum computation, *Phys. Rev. A* **69**, 062320 (2004)
- [87] D. I. Schuster, A. Wallraff, A. Blais, L. Frunzio, R.-S. Huang, J. Majer, S. M. Girvin, and R. J. Schoelkopf, ac Stark shift and dephasing of a superconducting qubit strongly coupled to a cavity field, *Phys. Rev. Lett.* **94**, 123602 (2005)
- [88] Alexandre Blais, Jay Gambetta, A. Wallraff, D. I. Schuster, S. M. Girvin, M. H. Devoret, and R. J. Schoelkopf, Quantum-information processing with circuit quantum electrodynamics, *Phys. Rev. A* **75**, 032329 (2007)
- [89] T. P. Orlando, J. E. Mooij, Lin Tian, Caspar H. van der Wal, L. S. Levitov, Seth Lloyd, J. J. Mazo, Superconducting persistent-current qubit, *Phys. Rev. B* **60**, 15398 - 15413 (1999)
- [90] J. E. Mooij, T. P. Orlando, L. Levitov, Lin Tian, Caspar H. van der Wal, and Seth Lloyd, Josephson Persistent-Current Qubit, *Science* **285**, 1036 (1999)
- [91] Caspar H. van der Wal, A. C. J. ter Haar, F. K. Wilhelm, R. N. Schouten, C. J. P. M. Harmans, T. P. Orlando, Seth Lloyd, and J. E. Mooij, Quantum Superposition of Macroscopic Persistent-

- Current States, *Science* **290**, 773 (2000)
- [92] I. Chiorescu, Y. Nakamura, C. J. P. M. Harmans, and J. E. Mooij, Coherent Quantum Dynamics of a Superconducting Flux Qubit, *Science* **299**, 1869 (2003)
- [93] Lev B. Ioffe, Vadim B. Geshkenbein, Mikhail V. Feigel'man, Alban L. Fauchère, Gianni Blatter, Environmentally decoupled sds -wave Josephson junctions for quantum computing, *Nature* **398**, 679-681 (1999)
- [94] J. M. Martinis, S. Nam, J. Aumentado, C. Urbina, Rabi Oscillations in a Large Josephson-Junction Qubit, *Phys. Rev. Lett.* **89**, 117901 (2002)
- [95] A. Cottet, D. Vion, A. Aassime, P. Joyez, D. Esteve, and M. H. Devoret, Implementation of a combined charge-phase quantum bit in a superconducting circuit *Physica C* **367**, 197 (2002)
- [96] G. Burkard, R. H. Koch, D. P. DiVincenzo, Multilevel quantum description of decoherence in superconducting qubits, *Phys. Rev. B* **69**, 064503 (2004)
- [97] G. Burkard, Circuit theory for decoherence in superconducting charge qubits, *Phys. Rev. B* **71**, 144511 (2005)
- [98] R. H. Koch, J. R. Rozen, G. A. Keefe, F. M. Milliken, C. C. Tsuei, J. R. Kirtley, and D. P. DiVincenzo, Low-bandwidth control scheme for an oscillator-stabilized Josephson qubit, *Phys. Rev. B* **72**, 092512 (2005)
- [99] G. Ithier, E. Collin, P. Joyez, P. J. Meeson, D. Vion, D. Esteve, F. Chiarello, A. Shnirman, Y. Makhlin, J. Schrieffer, and G. Schön, Decoherence in superconducting quantum bit circuit, *Phys. Rev. B* **72**, 134519 (2005)
- [100] L. Tian, L. S. Levitov, C. H. van der Wal, J. E. Mooij, T. P. Orlando, S. Lloyd, C. J. P. M. Harmans, and J. J. Mazo, Quantum mesoscopic phenomena and mesoscopic devices in microelectronics, edited by I. Kulik and R. Elliatoglu, NATO Science Series C: Mathematical and Physical Science No. 559 (Kluwer Academic, Dordrecht), p. 429 (2000)
- [101] P. Bertet, I. Chiorescu, C.J.P.M Harmans, J.E. Mooij, Dephasing of a flux-qubit coupled to a harmonic oscillator, arXiv:cond-mat/0507290 (2005)
- [102] P. Bertet, I. Chiorescu, G. Burkard, K. Semba, C. J. P. M. Harmans, D. P. DiVincenzo, and J. E. Mooij, Dephasing of a superconducting qubit induced by photon noise, *Phys. Rev. Lett.* **95**, 257002 (2005)
- [103] G. Burkard, D. P. DiVincenzo, P. Bertet, I. Chiorescu, and J. E. Mooij Asymmetry and decoherence in a double-layer persistent-current qubit, *Phys. Rev. B* **71**, 134504 (2005)
- [104] J. M. Martinis, S. Nam, J. Aumentado, and K. M. Lang, Decoherence of a superconducting qubit due to bias noise, *Phys. Rev. B* **67**, 094510 (2003)
- [105] O. Astafiev, Yu. A. Pashkin, Y. Nakamura, T. Yamamoto, and J. S. Tsai, Temperature square dependence of the low frequency $1/f$ charge noise in the Josephson junction qubits, *Phys. Rev. Lett.* **96**, 137001 (2006)
- [106] C. C. Yu, M. Constantin, and J. M. Martinis, Effect of two level system saturation on charge noise in Josephson junction qubits, arXiv:0707.1514 (2007)
- [107] R. H. Koch, D. P. DiVincenzo, and J. Clarke, Model for $1/f$ flux noise in SQUIDs and qubits, *Phys. Rev. Lett.* **98**, 267003 (2007)
- [108] F. Yoshihara, K. Harrabi, A. O. Niskanen, Y. Nakamura, and J. S. Tsai, Decoherence of flux qubits due to $1/f$ flux noise, *Phys. Rev. Lett.* **97**, 167001 (2006)
- [109] K. Kakuyanagi, T. Meno, S. Saito, H. Nakano, K. Semba, H. Takayanagi, F. Deppe, and A. Shnirman, Dephasing of a superconducting flux qubit, *Phys. Rev. Lett.* **98**, 047004 (2007)
- [110] Y. M. Galperin, B. L. Altshuler, J. Bergli, D. Shantsev, and V. Vinokur, Non-Gaussian dephasing in flux qubits due to $1/f$ noise, *Phys. Rev. B* **76**, 064531 (2007)
- [111] Y. M. Galperin, B. L. Altshuler, and D. V. Shantsev, Fundamental problems of mesoscopic physics, edited by I. V. Lerner et al. (Kluwer Academic Publishers, The Netherlands, 2004)
- [112] R. W. Simmonds, K. M. Lang, D. A. Hite, S. Nam, D. P. Pappas, and J. M. Martinis, Decoherence in Josephson phase qubits from junction resonators, *Phys. Rev. Lett.* **93**, 077003 (2004)
- [113] J. M. Martinis, K. B. Cooper, R. McDermott, M. Steffen, M. Ansmann, K. D. Osborn, K. Cicak, S. Oh, D. P. Pappas, R. W. Simmonds, and C.C. Yu, Decoherence in Josephson qubits from dielectric loss, *Phys. Rev. Lett.* **95**, 210503 (2005)
- [114] R. C. Bialczak, R. McDermott, M. Ansmann, M. Hofheinz, N. Katz, E. Lucero, M. Neeley, A. D. O'Connell, H. Wang, A. N. Cleland, and J. M. Martinis, $1/f$ flux noise in Josephson phase qubits, *Phys. Rev. Lett.* **99**, 187006 (2007)
- [115] A. Shnirman, G. Schön, I. Martin, and Y. Makhlin, Low- and high-frequency noise from coherent two-level systems, *Phys. Rev. Lett.* **94**, 127002 (2005)
- [116] S. Hunklinger and A. K. Raychaudhuri, *Amorphous Solids: Low-Temperature Properties* ed. by

W. A. Phillips (Springer, Berlin, 1981)